Numerical Study of Blowup Problems and Conservation Laws with Moving Mesh Methods

by

Jianping Chen

B. Sc., The University of Science and Technology of China, 1987

A THESIS SUBMITTED IN PARTIAL FULFILLMENT
OF THE REQUIREMENTS FOR THE DEGREE OF
MASTER OF SCIENCES
in the Department
of
Mathematics and Statistics

SIMON FRASER UNIVERSITY
August 1996

ISBN 0-612-16831-X

PARTIAL COPYRIGHT LICENSE

I hereby grant to Simon Fraser University the right to lend my thesis, project or extended essay (the title of which is shown below) to users of the Simon Fraser University Library, and to make partial or single copies only for such users or in response to a request from the library of any other university, or other educational institution, on its own behalf or for one of its users. I further agree that permission for multiple copying of this work for scholarly purposes may be granted by me or the Dean of Graduate Studies. It is understood that copying or publication of this work for financial gain shall not be allowed without my written permission.

Title of Thesis/Project/Extended Essay

Numerical Study of Blowup Problem and Conservation Laws with Moving Mesh Methods

Author:

(signature) /

(name)

Aug 8, 1996

(date)

APPROVAL

Name: Jianping Chen

Degree: Master of Sciences

Title of thesis: Numerical Study of Blowup Problems and Conservation laws with Moving Mesh Methods

Examining Committee: Dr. Carl Schwarz
Chair

Dr. Robert D. Russell,
Senior Supervisor

Dr. Keith Promislow

Dr. Tao Tang

Dr. Manfred Trummer, External Examiner

Date Approved: August 19, 1996

Abstract

Moving mesh methods have been shown to be successful in last few years for time-dependent partial differential equations with large solution variations, especially for blowup problems. In this thesis, we use the moving mesh methods based on moving mesh PDEs to study a few blowup problems and conservation laws. In chapter 1, we briefly go through the development of the methods. The equidistribution principle, from which the moving mesh PDEs are deduced, is introduced. In chapter 2, studies of the blowup problems are carried out. Some of the formal analysis of the problems is compared with our computations to show the performance of the method. In chapter 3, the methods are used on conservation laws, where discontinuous solutions and large variations in the first derivatives are expected. It is shown that, with proper spatial discretization, the moving mesh methods implicitly adapt the artificial viscosity while other spatial discretizations may fail to give physical solutions. Some of the problems encountered are discussed. New adaptive Godunov type schemes for conservation laws are developed and the performance of this approach is demonstrated by computations. We give a summary of the conclusions and remarks in chapter 4. Some ideas for future study are also suggested.

Acknowledgments

I would like to deeply thank my supervisor, Dr. Robert D. Russell for his patience, guidance, and encouragement during my study here.

Special thanks go to Dr. Weizhang Huang for his kind help.

I would also like to give my special thanks to Dr. Keith Promislow for his instructive suggestions and his patience reading my manuscripts.

The author is grateful for the continuing support of the Department of Mathematics and Statistics, Simon Fraser University.

Dedication

To my mother, Ms. *Zi-An Deng*, who led me into mathematics in my early childhood.

Contents

List of Tables

List of Figures

Chapter 1

Moving Mesh Methods

1.1 Method of Lines

When considering the time-dependent PDE initial-boundary value problem:

$$u_t = f(u), \qquad a < x < b, \quad 0 < t < T, \tag{1.1}$$

$$u(x,0) = g(x), \qquad a < x < b \tag{1.2}$$

where f is a first or second order spatial differential operator with suitable boundary conditions at a and b, we have two common approaches to compute the numerical solution. The first is to discretize the PDE both in time and space, usually on a fixed uniform spatial mesh. This method changes the PDE into an algebraic system by replacing the partial derivatives with finite differences. We obtain the numerical solution by solving the resulting algebraic system. Another approach is the so called *method of lines (MOL)* approach or semi-discrete method. In this approach, we discretize the PDE in space or in time only. In the transverse method of lines, we discretize in time and get a system of ODEs in spatial variables with boundary conditions, i.e., an ODE boundary value problem. Discretization in space leads us to a system of ODEs with initial conditions. The numerical solution can be obtained by solving the ODE initial value problems. The latter is often referred to as the longitudinal method of lines.

The possible advantages of MOL are:

1. By separating the problems of space and time discretization it is easy to establish stability and convergence.

2. The powerful numerical techniques for solving ODEs, such as dynamical regridding of the stepsize which maintains stability and desired time integration accuracy, can be directly applied to the PDE case. Existing ODE software neatly reduces programming effort.

3. Using an MOL approach, one needs only be concerned with discretizing spatial derivatives. Solving the ODEs very accurately permits comparison of the accuracy and efficiency of different approximations of spatial derivatives.

The possible disadvantages of an MOL approach are that the reduced ODEs may become very stiff and overall optimization of the method may be lost by decoupling the analysis of the space and time discretization.

This method of lines approach, which separates the spatial and temporal variables makes possible the use of different meshes at different time levels. It is our goal to exploit this property of the method of lines approach to develop adaptive mesh methods and apply them to a selection of scalar degenerate blowup problems, a nonlinear coupled system, and scalar conservation laws.

1.2 Moving Mesh Methods

It has been amply demonstrated that significant improvements in accuracy and efficiency can be gained by adapting mesh points so that they are concentrated about areas of large solution variation. For problems with large solution variations, viz. shock waves, layers, and single point blowup, constructing an adaptive mesh in time can be essential if the problem is to be solved efficiently, and often if it is to be solved at all.

There are many ways to adapt the meshes. The two most popular are:

1. Local refinement methods:

   Mesh points are added or deleted according to the profile of the solution and the local errors.

2. Moving mesh methods:

   A fixed number of mesh points move adaptively to minimize a selected monitor function which is an estimation of the errors of the solution.

A combination of the two methods is also possible [1].

A difficulty with local refinement methods for certain problems, e.g. those with a single point blowup, is that the total number of the mesh points may increase drastically, compounding the difficulty of the computation [6]. Moving mesh methods are especially attractive for this kind of problems, and they will be the focus of our attention in the sequel.

Almost all moving mesh methods are based on a Lagrangian type approach which is best introduced via a co-ordinate transformation. Considering the PDE (1.1), let (ξ, t) be new independent variables linked with the old independent variables (x, t) through a co-ordinate transformation $x = x(\xi, t)$. Denoting $v(\xi, t) = u(x, t)$, the total derivative of v is $\partial v/\partial t = \partial u/\partial x \; \partial x/\partial t + \partial u/\partial t$, and the Lagrangian form of (1.1) reads

$$\frac{\partial v}{\partial t} = \frac{\partial u}{\partial x}\frac{\partial x}{\partial t} + f(v), \quad \xi_a < \xi < \xi_b, \quad 0 < t < T. \tag{1.3}$$

The basic idea of the Lagrangian approach is to choose the variables (ξ, t) so that the problem is easier to handle numerically than for the original pair (x, t). For equations with large variation in solutions, a standard MOL approach in original variables (x, t) would require the ODE solver to take small time steps to maintain stability. With the above Lagrangian approach, ideally, if a suitable nonuniform x-grid exists according to the change of variables $x = x(\xi, t)$, we can then take acceptable step sizes in the time direction while using a coarse uniform ξ-grid in space. The variables (x, t) and (ξ, t) are called the physical and the computational co-ordinate variables respectively.

Moving mesh methods can be roughly divided into two categories: static and dynamic. In the static approach [32], each time step consists of two computational stages: a step involving the application of a stiff ODE solver to an augmented semi-discrete system, followed by a second regridding stage in which a redistribution of points at the forward time level is carried out and the solution is then interpolated to the new mesh. Although it is highly reliable and robust, the very frequent regriddings prevent the integration procedure from exploiting the attractive, higher order BFD formulas of the ODE solver and interpolations can cause perceptible loss of spatial accuracy [18].

Among moving mesh methods, the moving finite element methods developed by Miller and his co-workers [36], [37], [38] are perhaps more elegantly formulated in mesh movement than moving finite difference methods. However, their methods require properly choosen parameters, which are highly problem dependent, to ensure proper governing of the mesh,

and some measures have to be taken to avoid node overtaking and singular mass matrices [18]. In contrast, one of the objectives in the recent development of the moving finite difference methods is to uncover a mechanism to select the spatial mesh more automatically. Moving finite element methods are beyond the scope of this thesis, and a more detailed analysis can be found in [4], [5] and [48].

In this study, we take a dynamic approach for the moving mesh based on the idea of Dorfi and Drury [14] which is recommended in [18] for its simplicity and insensitivity to the parameters. With a moving mesh approach, we augment the physical equation (1.3) with a moving mesh equation, which will be detailed in the next section. The system in Lagrangian co-ordinate variables is solved by a stiff ODE solver, DDASSL [41]. Because the solution and the mesh can be solved simultaneously, no regridding and interpolation is necessary, and the integration of the ODE solver will not be interrupted so that we can benefit, to a large extend, from the efficiency of the ODE solver.

1.3 Equidistribution Principle and Moving Mesh PDEs

In computations with moving mesh methods, the most important consideration is the decision of how to automatically and stably choose a nonuniform mesh which suitably adapts to the solution behavior. Unfortunately, the resolution of this issue has been proven to be very difficult. Although a few mesh selection principles have been suggested in the literature [18], [25], [32], the problem of which overall strategy to use and how to best choose the mesh for a given strategy is still controversial [18].

Among various moving mesh methods, the most popular is based on the idea of equidistribution first introduced by de Boor [9] and Dodson [13]. A number of moving mesh methods have been developed in the literature [1], [2], [16], [26], [27], [44], [45], and almost all are based on the equidistribution principle.

The idea behind the equidistribution principle is that if some measure of error $M(x)$, also called the monitor function, is available, then a good choice of a mesh $\pi : a = x_0 < x_1 < \cdots < x_N = b$ would be one for which the contributions to the error over the subintervals are equally distributed. Without loss of generality, we assume the computational coordinate ξ is in the unit interval $[0, 1]$ and a uniform mesh is given on the computational domain by

$$\xi_i = \frac{i}{n}, \quad i = 0, 1, \ldots, n.$$

In the one dimensional case, for a chosen monitor function $M(x,t)$ (> 0), the equidistribution principle can be expressed in its integral form [43] as:

$$\int_a^{x(\xi,t)} M(\tilde{x},t)d\tilde{x} = \xi\theta(t) \tag{1.4}$$

where

$$\theta(t) = \int_a^b M(\tilde{x},t)d\tilde{x}.$$

By differentiating (1.4), several MMPDEs have been derived in [28] based on the equidistribution principle. In the following, we briefly go through their derivation for completeness and for future reference.

Differentiating (1.4) with respect to ξ once and twice, we obtain

$$M(x(\xi,t),t)\frac{\partial}{\partial\xi}x(\xi,t) = \theta(t)$$

and

$$\frac{\partial}{\partial\xi}\{M(x(\xi,t),t)\frac{\partial}{\partial\xi}x(\xi,t)\} = 0, \tag{1.5}$$

respectively.

By differentiating (1.5) with respect to time t and expanding, we have:

$$(MMPDE1) \qquad \frac{\partial}{\partial\xi}(M\frac{\partial\dot{x}}{\partial\xi}) + \frac{\partial}{\partial\xi}(\frac{\partial M}{\partial\xi}\dot{x}) = -\frac{\partial}{\partial\xi}(\frac{\partial M}{\partial t}\frac{\partial x}{\partial\xi}). \tag{1.6}$$

The moving mesh methods used in [12], [16], [44], and [45] are equivalent to or closely related to (1.6). In (1.6), $\frac{\partial M}{\partial t}$ can be regarded as the source of the mesh movement [28]. Unfortunately, in actual applications $\frac{\partial M}{\partial t}$ is often hard or impossible to compute.

Instead of requiring that the mesh satisfy (1.6) at time t, we may require that (1.5) is satisfied at a later time $t+\tau$, i.e.,

$$\frac{\partial}{\partial\xi}\{M(x(\xi,t+\tau),t+\tau)\frac{\partial}{\partial\xi}x(\xi,t+\tau)\} = 0. \tag{1.7}$$

This can be regarded as a condition to regularize the mesh movement.

By using the second order expansion and dropping the higher order terms in (1.7), we obtain

$$(MMPDE2) \qquad \frac{\partial}{\partial\xi}(M\frac{\partial\dot{x}}{\partial\xi}) + \frac{\partial}{\partial\xi}(\frac{\partial M}{\partial\xi}\dot{x}) = -\frac{\partial}{\partial\xi}(\frac{\partial M}{\partial t}\frac{\partial x}{\partial\xi}) - \frac{1}{\tau}\frac{\partial}{\partial\xi}(M\frac{\partial x}{\partial\xi}). \tag{1.8}$$

Compared with (1.6), (1.8) contains the additional term

$$-\frac{1}{\tau}\frac{\partial}{\partial\xi}(M\frac{\partial x}{\partial\xi}),$$

which implies that in (1.8) some deviation from equidistribution is acceptable.

Two other MMPDEs based on (1.8) in [28] are

$$(MMPDE3) \qquad \frac{\partial^2}{\partial\xi^2}(M\dot{x}) = -\frac{1}{\tau}\frac{\partial}{\partial\xi}(M\frac{\partial x}{\partial\xi}), \tag{1.9}$$

and

$$(MMPDE4) \qquad \frac{\partial}{\partial\xi}(M\frac{\partial\dot{x}}{\partial\xi}) = -\frac{1}{\tau}\frac{\partial}{\partial\xi}(M\frac{\partial x}{\partial\xi}). \tag{1.10}$$

Anderson [2] derived another moving mesh PDE:

$$(MMPDE5) \qquad \dot{x} = \frac{1}{\tau}\frac{\partial}{\partial\xi}(M\frac{\partial x}{\partial\xi}), \tag{1.11}$$

based on attraction and repulsion pseudoforces.

In [1] Adjerid and Flaherty used a method equivalent to the discrete form of

$$(MMPDE6) \qquad \frac{\partial^2\dot{x}}{\partial\xi^2} = -\frac{1}{\tau}\frac{\partial}{\partial\xi}(M\frac{\partial x}{\partial\xi}). \tag{1.12}$$

Remarks:

1. In the above derivation, the process of differentiation implicitly assumes that $x(\xi,t)$ nearly satisfies (1.5) which is generally not always true in actual computations.

2. Almost all MMPDEs are obtained without considering the physical properties of the phenomena modelled by the physical equation. However, information about the physical situation may be recorded through a properly chosen monitor function, as demonstrated in next chapter.

1.4 Moving Collocation Method

In this section, we give a detailed explanation of the moving collocation method, used to study so-called blowup problems. A different numerical method will be used in chapter 3 to study conservation laws.

It is known that moving mesh methods can be unstable, and some sort of smoothing of the mesh is often necessary in order to obtain non-oscillatory, accurate solutions. Actually,

(1.7), which leads to MMPDE2, 3, 4, and 6, can also be regarded as a kind of temporal smoothing, where the relaxation time τ controls the speed of the mesh. As for spatial smoothing, instead of the monitor function M, a smoothed monitor function defined by

$$\tilde{M} - \frac{1}{\lambda^2}\frac{\partial^2 \tilde{M}}{\partial \xi^2} = M \tag{1.13}$$

is used in the moving mesh equations. Replacing M in (1.10) with $\tilde{M}$ and using (1.13), we get

$$\frac{\partial}{\partial \xi}\left\{\frac{\left(I - \frac{1}{\lambda^2}\frac{\partial^2}{\partial \xi^2}\right)\frac{1}{\frac{\partial x}{\partial \xi}+\frac{1}{\tau}\frac{\partial x}{\partial \xi}}}{M}\right\} = 0. \tag{1.14}$$

The smoothed moving mesh equation (1.14) has some desired properies. It has been proven in [30] that (1.14) and its discrete analogue leads to longterm regularity of the mesh, no node-crossing will occur and the level of perturbation from equidistribution decreases.

In actual computations, a moving collocation approach, motivated by the idea that the mesh points do not need to be resolved with the same accuracy as the solution to the PDE itself, is used. In this approach, the MMPDEs are discretized in ξ with 3-point finite differences on a uniform mesh, the physical PDE(s) are discretized in x with Hermite cubic collocation on the corresponding nonuniform mesh, and the resulting system is then integrated.

Consider a second-order parabolic PDE in divergence form [31]

$$F(t, x, u, u_x, u_t, u_{xx}) = \frac{\partial}{\partial x}G(t, x, u, u_x, u_t, u_{xt}), \quad x_L(t) < x < x_R(t), \quad 0 < t < T. \tag{1.15}$$

In the collocation method, for a given mesh $x_1(t) := x_L(t) < x_2(t) < \cdots < x_R(t) := x_N(t)$, the solution $u(x,t)$ for $x \in [x_i(t), x_{i+1}(t)], i = 1, \ldots, N-1$ is approximated by

$$v(x,t) = v_i(t)\psi_1(s^{(i)}) + v_{x,i}(t)H_i(t)\psi_2(s^{(i)}) + v_{i+1}(t)\psi_3(s^{(i)}) + v_{x,i+1}(t)H_i(t)\psi_4(s^{(i)}),$$

where $v_i(t)$ and $v_{x,i}(t)$ denote approximations to $u(x_i(t),t)$ and $u_x(x_i(t),t)$, respectively,

$$s^{(i)} := (x - x_i(t))/H_i(t), \quad H_i(t) := x_{i+1}(t) - x_i(t),$$

and the ψ_i's are the standard shape functions of cubic Hermite interpolation.

Taking a cell average for (1.15) on each half of $[x_i, x_{i+1}]$, we get

$$\int_{x_i}^{(x_i+x_{i+1})/2} F dx = G_{i+1/2} - G_i, \qquad \int_{(x_i+x_{i+1})/2}^{x_{i+1}} F dx = G_{i+1} - G_{i+1/2}, \tag{1.16}$$

where

$$G_i := G\,|_{(x_i,t)}, \quad G_{i+1/2} := G\,|_{((x_i+x_{i+1})/2,t)}, \quad G_{i+1} := G\,|_{(x_{i+1},t)}\,.$$

Approximating F piecewise linearly

$$F \approx F\,|_{(x_{i1},t)}\,(x-x_{i2})/(x_{i1}-x_{i2}) + F\,|_{(x_{i2},t)}\,(x-x_{i1})/(x_{i2}-x_{i1}),$$

in (1.16), where x_{i1} and x_{i2} are two collocation points given by

$$x_{i1}(t) := x_i(t) + s_1 H_i(t), \quad x_{i2}(t) := x_i(t) + s_2 H_i(t), \tag{1.17}$$

$$s_1 := 0.5(1-1/\sqrt{3}), \quad s_2 := 0.5(1+1/\sqrt{3}), \tag{1.18}$$

and integrating with the two point Gauss quadrature formula, we have

$$\begin{aligned} F|_{(x_{i1},t)}H_i(2s_2-0.5)/4(s_2-s_1) + F|_{(x_{i2},t)}H_i(0.5-2s_1)/4(s_2-s_1) &= G_{i+1/2}-G_i, \\ F|_{(x_{i2},t)}H_i(2s_2-1.5)/4(s_2-s_1) + F|_{(x_{i2},t)}H_i(1.5-2s_1)/4(s_2-s_1) &= G_{i+1}-G_{i+1/2}. \end{aligned} \tag{1.19}$$

Solving for $F\,|_{(x_{i1},t)}$ and $F\,|_{(x_{i2},t)}$ in (1.19) using (1.18), we get the collocation discretization of the physical equation (1.15):

$$\begin{aligned} F\,|_{(x_{i1},t)} &= (1/H_i)\left(-(1+2/\sqrt{3})G_i + (4/\sqrt{3})G_{i+1/2} + (1-2/\sqrt{3})G_{i+1}\right), \\ F\,|_{(x_{i2},t)} &= (1/H_i)\left(-(1-2/\sqrt{3})G_i - (4/\sqrt{3})G_{i+1/2} + (1+2/\sqrt{3})G_{i+1}\right). \end{aligned}$$

From the smoothing of the monitor function (1.13), we have

$$\tilde{M} = \left(I - \lambda^{-2}\frac{\partial^2}{\partial\xi^2}\right)^{-1} M.$$

With properly chosen λ,

$$\left(I-\lambda^{-2}\Delta\right)^{-1} \approx I + \lambda^{-2}\Delta + (\lambda^{-2}\Delta)^2 + \cdots + (\lambda^{-2}\Delta)^p,$$

where $\Delta = \frac{\partial^2}{\partial\xi^2}$. It is argued in [30] and [29] that, with centered finite difference approximation for Δ, i.e. $\Delta M \approx \frac{M_{i+1}-M_{i-1}}{x_{i+1}-x_{i-1}}$, the smoothed monitor function can be computed by a suitable combination of neighbouring values of M. Here we use

$$\tilde{M}_i = \sqrt{\frac{\sum_{k=i-p}^{i+p}(M_k)^2\left(\frac{\gamma}{1+\gamma}\right)^{|k-i|}}{\sum_{k=i-p}^{i+p}\left(\frac{\gamma}{1+\gamma}\right)^{|k-i|}}}, \tag{1.20}$$

where γ is a smoothing parameter[30]. Usually we take $\gamma = 2$, and p is a nonnegative integer which we often refer to as the smoothing index ip in following chapters. The summations in (1.20) are understood to contain only those elements with indices in the range of zero and the number of mesh points used. The moving mesh equations are discretized by 3-point finite differences. For example, the discretization of (1.14) is

$$\frac{1}{(1/n)^2}(\dot{x}_{i+1} - 2\dot{x}_i + \dot{x}_{i-1}) = -\frac{1}{\tau}\left[\frac{\tilde{M}_{i+1} + \tilde{M}_i}{2(1/n)^2}(x_{i+1} - x_i) - \frac{\tilde{M}_i + \tilde{M}_{i-1}}{2(1/n)^2}(x_i - x_{i-1})\right].$$

Chapter 2

Numerical Study of Blowup Problems

Many partial differential equations modelling physical phenomena have solutions which blow up (become infinite) in a finite time. The equations are basically of reaction-diffusion type arised from combustion theory and thermodynamics. These models with some applications [22], for example, in the study of spontaneous ignition used by the loss adjustors, have raised a lot of research and pratical interest in last twenty years.

One feature of this type of singularity is that as the blowup time T is approached, changes in the solution occur on increasingly smaller length scales and on increasingly smaller time scales. When the length scale of the singularity approaches that of the spacing between mesh points, the accuracy of a fixed mesh computation will diminish significantly. To compute such singular behaviour accurately, it is essential to use a numerical method which adapts the spatial mesh as the singularity develops.

In this chapter, we use the moving collocation method developed in the previous chapter to study a few problems with blowup phenomena.

2.1 Degenerate Blowup Problems

In [10], it has been shown that moving mesh methods developed in [29] are efficient and successful in resolving the spatial feature of the blowup problem

$$u_t = u_{xx} + u^p, \quad p > 1. \tag{2.1}$$

In this section we study a model for a fluid in a channel with a temperature dependent source derived by Ockendon [39]:

$$x^q u_t = u_{xx} + u^p, \tag{2.2}$$

$$u(0,t) = u(1,t) = 0, \tag{2.3}$$

$$u(x,0) = u_0(x) > 0. \tag{2.4}$$

In Floater [17], it is shown that if $u_0(x)$ is sufficiently large then the solution of (2.2) blows up and that if $p \leq q+1$ the blowup point is at the origin so that there is a sequence $x_*(t) \to 0$ such that $u(x_*(t),t) \to \infty$ as $t \to T$ where T is the blowup time. It is conjectured that if $p > q+1$ then blow-up occurs at an interior point $x_* \neq 0$. Accordingly we examine the two cases $q = 2, p = 3$ and $q = 1, p = 3$. The emphasis here is to resolve the blowup structure without exploiting the analytic results.

2.1.1 Blowup at the origin when $q = 2, p = 3$

Assuming the blowup point x_b is the origin, the equation (2.2) is invariant under the rescaling

$$\begin{aligned} T - \bar{t} &= \lambda(T-t), \\ \bar{u} &= \lambda^{-\frac{2}{(q+2)(p-1)}} u, \\ \bar{x} - x_b &= \lambda^{\frac{1}{q+2}}(x - x_b), \end{aligned} \tag{2.5}$$

and a natural set of variables to use are coordinates related to the rescaling with $q = 2, p = 3$. Accordingly we set

$$s = -\log(T-t), \quad y = (T-t)^{-\frac{1}{4}} x, \quad w(y,s) = u(T-t)^{\frac{1}{4}}, \tag{2.6}$$

Under this change of variables, (2.2)-(2.4) becomes

$$w_s = w_{yy} - \frac{y^2}{4}(y w_y + w) + w^3, \tag{2.7}$$

$$w(0,s) = 0, \qquad w(y,s) \to \frac{K}{y}, \quad y \to \infty,$$

where K is a constant.

First we look for an analytic asymptotic form for the blowup. Following the method adapted in [6], we seek an approximately self-similar solution in the form

$$w = g(s) f(z), \quad \text{where} \quad z = \frac{y}{g(s)}. \tag{2.8}$$

To allow a consistent asymptotic expression we require that

$$g(s) \to \infty, \quad s \to \infty. \tag{2.9}$$

Using (2.8), (2.7) reads

$$-\frac{z^2}{4}(zf_z + f) + f^3 = -g^{-4}f_{zz} + \dot{g}g^{-3}(f - zf_z). \tag{2.10}$$

For large s (t close to T), (2.9) implies that (2.10) reduces to

$$-\frac{z^2}{4}(zf_z + f) + f^3 = 0, \tag{2.11}$$

whose solution is

$$f(z) = \frac{1}{\sqrt{2}}\frac{z}{\sqrt{1+z^4}}, \tag{2.12}$$

and considering higher order terms in (2.10) to the leading order, we get

$$g(s) = As^{\frac{1}{4}}, \tag{2.13}$$

where A is a constant. Combining the above results we get the conjectured asymptotic solution profile for u:

$$v(x,t) = \frac{1}{\sqrt{2}}(T-t)^{-\frac{1}{2}}\frac{x}{\sqrt{1+\frac{x^4}{A^4(T-t)|\log(T-t)|}}}, \tag{2.14}$$

which in turn implies that the maximum value of v is

$$v_{\max}(t) = \frac{1}{2}(T-t)^{-\frac{1}{4}} \cdot A|\log(T-t)|^{\frac{1}{4}}, \tag{2.15}$$

the maximum point of the asymptotic solution is

$$x_*(t) = (T-t)^{\frac{1}{4}} \cdot A|\log(T-t)|^{\frac{1}{4}}, \tag{2.16}$$

and

$$v_x(0,t) = \frac{1}{\sqrt{2}}(T-t)^{-\frac{1}{2}}. \tag{2.17}$$

To corroborate the above conjectured solution, we compute the solution of (2.2) with initial data $u_0(x) = 20\sin\pi x$ and the following parameters: $\tau = 10^{-7}$ in MMPDE6 (1.12), smoothing index $ip = 1$ which means a three point averaging for spatial smoothing, absolute error tolerance $rtol = 10^{-9}$ and relative error tolerance $atol = 10^{-5}$ for the ODE solver

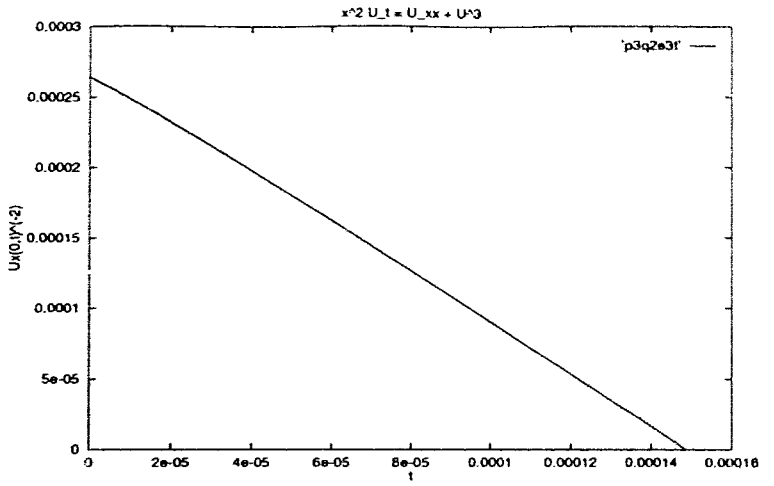

Figure 2.1: $u_x(0,t)$ *as a function of* $T-t$

DDASSL. It has been shown in [10] that for the success of the computation it is important to choose a monitor function which preserves the scaling invariance. We choose

$$M = u^{\frac{(q+2)(p-1)}{2}} \tag{2.18}$$

which makes (1.12) invariant under (2.5). Actually, no choice of monitor functions of the form $M(u, u_x)$ can make other moving mesh equations listed in section 1.3 invariant under (2.5) if τ is kept constant. For $q = 2, p = 3$, (2.18) reduces to $M = u^4$.

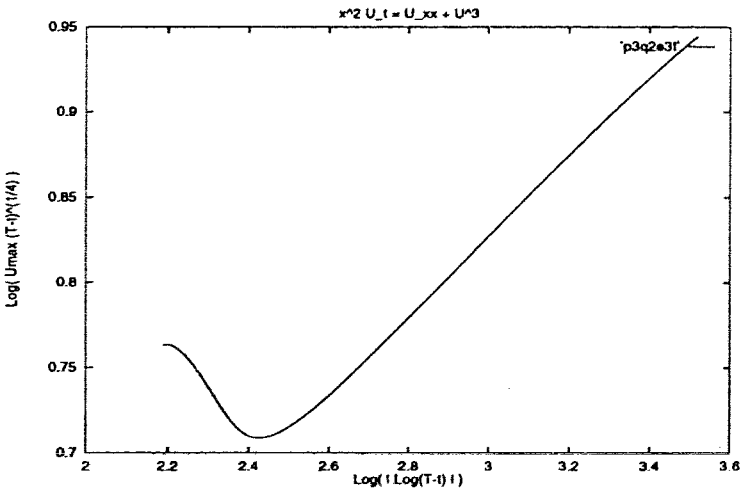

Figure 2.2: *Relationship between* $u_{\max}$ *and* $T-t$

From (2.17), we have

$$v_x(0,t)^{-2} = 2(T-t) \tag{2.19}$$

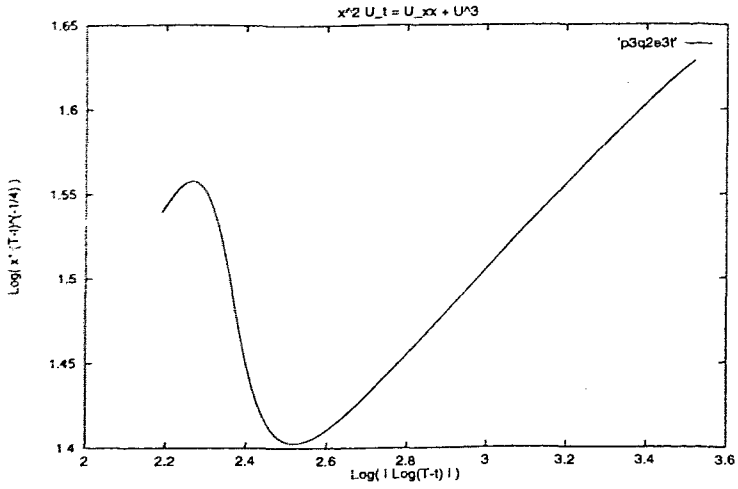

Figure 2.3: *Relationship between x_* and $T-t$*

which implies that if $u_x(0,t)^{-2}$ is plotted as a function of time t, the result should be a straight line with slope -2. This is confirmed in figure 2.1. In principle, this output can be used to estimate the blowup time T.

From (2.15), we readily obtain

$$\log\left(v_{\max}\cdot(T-t)^{\frac{1}{4}}\right)=\frac{1}{4}\log\left(|\log(T-t)|\right)+c, \tag{2.20}$$

where c is a constant. In figure 2.2, we plot $\log\left(u_{\max}(T-t)^{\frac{1}{4}}\right)$ versus $\log(|\log(T-t)|)$ based on the estimate $T-t=1/2\cdot u_x(0,t)^{-2}$ from (2.17). Clearly, near the blowup time (2.20) holds, i.e., our computation matches the magnitude of the solution near blowup time.

In figure 2.3, $\log\left(x_*(T-t)^{-\frac{1}{4}}\right)$ is plotted against $\log(|\log(T-t)|)$. Comparing with (2.16), it demonstrates that our computation captured the blowup point accurately.

From (2.14) and (2.16), we can find that

$$\frac{v(\xi x_*,t)}{v_{\max}}=\sqrt{2}\frac{\xi}{\sqrt{1+\xi^4}}=:h(\xi) \tag{2.21}$$

is independent of time. This implies that the spatial feature of the solution, as described by (2.21), is independent of time near blowup time T. In figure 2.4, we present $u/u_{\max}$ as a function of $\xi=x/x_*$ for times when $u_{\max}=1.2\times10^4, 6\times10^3, 3\times10^3, 1.5\times10^3, 7.5\times10^2, 3.75\times10^2$. It demonstrates reasonable convergence towards (2.21).

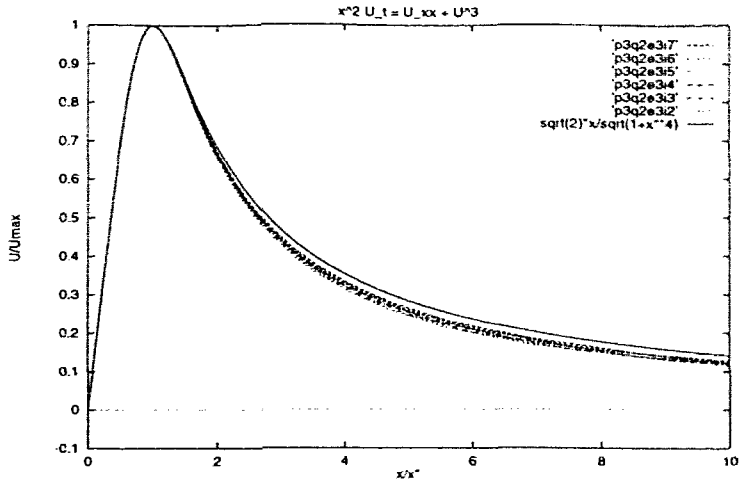

Figure 2.4: *Asymptotic solution profile as a function of* x/x^*

2.1.2 Blow up at an interior point when $q = 1, p = 3$

In this case, close to the blowup point, the equation (2.2) effectively becomes

$$(x_b)^q u_t = u_{xx} + u^p, \tag{2.22}$$

which is invariant, with the absence of boundary conditions, under the rescaling:

$$\begin{aligned} T - \bar{t} = &\quad \lambda(T - t), \\ \bar{u} = &\quad \lambda^{-\frac{1}{(p-1)}} u, \\ \bar{x} - x_b = &\quad \lambda^{\frac{1}{2}}(x - x_b), \end{aligned} \tag{2.23}$$

where x_b is the blowup point.

MMPDE6 (1.12) is invariant under (2.23) if

$$M = u^{p-1}. \tag{2.24}$$

Therefore, we use this as our monitor function.

In [10], it was shown that close to the peak the computed solution $U(\xi, t)$ and coordinate transformation $x(\xi, t)$ for (2.1) can be represented as

$$U(\xi, t) = (T - t)^{-\frac{1}{(p-1)}} W(\xi), \quad x(\xi, t) = x_b + (T - t)^{\frac{1}{2}} |\log(T - t)|^{\frac{1}{2}} y(\xi), \tag{2.25}$$

where $W(\xi)$ and $y(\xi)$ are independent of time t. For the case $q = 1, p = 3$,

$$W(\xi) = \frac{1}{\sqrt{2}}(x_b)^{\frac{1}{2}} \cos(\pi(\xi - \frac{1}{2})), \tag{2.26}$$

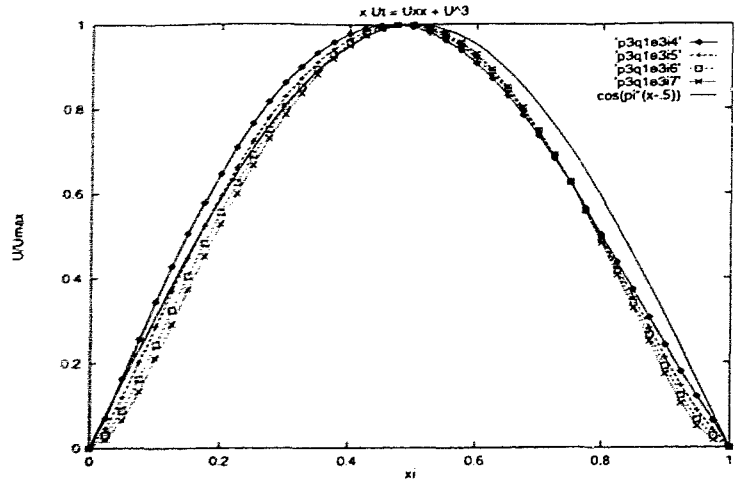

Figure 2.5: *Scaled solution as a function of the computational coordinate*

$$y(\xi) = 2\sqrt{\frac{2}{3}}(x_b)^{-\frac{1}{2}} \tan(\pi(\xi - \frac{1}{2})),$$

which implies that, as a function of the computational variables, the scaled solution $u/u_{\max}$ has the asymptotic form $\cos(\pi(\xi - 1/2))$.

In figure 2.5, we present this scaled numerical solution obtained using a smoothed version $\tilde{M}$ of the monitor function. In the computation, we used 41 mesh points, the smoothing index $ip = 1$, temperal smoothing parameter $\tau = 10^{-5}$, and the error tolerance for DDASSL $atol = rtol = 10^{-8}$. with initial condition $u_0(x) = 100\sin(\pi x)$. The result appears to deviate from the profile given in (2.26). This can be accounted for by the fact that the analysis was carried out for (2.22) (which is an approximation of (2.2)!), but the computation was done for (2.2) itself.

Worth noting is that, with different initial conditions, no obvious change in the spatial feature as a function of the computational coordinate was observed, but the blowup point (in the *physical* coordinate) does change, as shown in figure 2.6 where the resulting spatial profiles when $\|u\|_\infty = 1.6 \times 10^4$ are given. The relationship between local structure of the initial condition and the blowup point is not yet clear.

There is evidence showing that blow-up time is closely related to the L^2 norm rather than the infinity norm $\|\cdot\|_\infty$ of the initial conditions. In principle, the numerical method could be used to reliably determine x_b and T as functions of the initial data, but we do not do this here since no rigorous analytic results can be used to compare with.

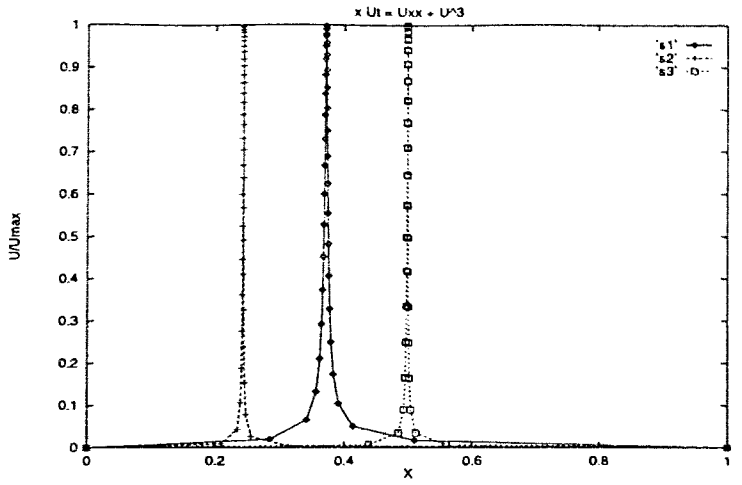

Figure 2.6: *Blowup point changes for several different initial conditions: s1:* $100\sin(\pi x)$, *s2:* $100x(1-x)e^{-x}$, *s3:* $100x(1-x)e^{-(1-x)}$

2.2 A Blowup System

In this section, we consider a blowup system defined by:

$$\begin{aligned} u_t &= u_{xx} + v^p, \\ v_t &= v_{xx} + u^q \end{aligned} \tag{2.27}$$

with

$$\begin{aligned} u(x,0) &= u_0(x) > 0, \\ v(x,0) &= v_0(x) > 0, \end{aligned}$$

modelling heat propagation in a two-component combustible mixture. This system has been studied by Escobedo and Herrero and others (cf. [15] and references therein). It has been shown in [15] that when $pq > 1$ and $(\gamma+1)/(pq-1) \geq N/2$ with $\gamma = \max\{p,q\}$ and N is the dimension in space, nontrivial solutions of (2.27) blow up in finite time. In this study, we shall restrict our attention to the one-dimensional case, i.e., $N = 1$. Since to the author's knowledge little is known about the solution behavior of (2.27) and virtually no computation has been done, we will first carry out a formal analysis, and some computational results will be compared with the analytic calculation.

2.2.1 A Formal Analysis

The system (2.27) is invariant under the transformation:

$$\begin{aligned} T-\bar{t} &= \lambda(T-t), \\ \bar{x}-x^* &= \lambda^{1/2}(x-x^*), \\ \bar{u} &= \lambda^{-(p+1)/(pq-1)}u, \\ \bar{v} &= \lambda^{-(q+1)/(pq-1)}v, \end{aligned} \tag{2.28}$$

where x^* is the blowup point. Since $u(T-t)^{(p+1)/(pq-1)}$ and $v(T-t)^{(q+1)/(pq-1)}$ are invariant under (2.28), we can assume

$$u(x,t) = (T-t)^{-(p+1)/(pq-1)}f(y,s) \tag{2.29}$$

$$v(x,t) = (T-t)^{-(q+1)/(pq-1)}g(y,s) \tag{2.30}$$

where

$$\begin{aligned} y &= (x-x^*)(T-t)^{-1/2}, \\ s &= -log(T-t). \end{aligned} \tag{2.31}$$

Then (2.27) becomes

$$\begin{aligned} (p+1)/(pq-1)f + f_s + 1/2f_y &= f_{yy} + g^p, \\ (q+1)/(pq-1)g + g_s + 1/2g_y &= g_{yy} + f^q, \end{aligned} \tag{2.32}$$

which has the constant solutions

$$\begin{aligned} f = \beta_1 &= \frac{(p+1)^{\frac{1}{pq-1}}(q+1)^{\frac{p}{pq-1}}}{(pq-1)^{\frac{p+1}{pq-1}}}, \\ g = \beta_2 &= \frac{(q+1)^{\frac{1}{pq-1}}(p+1)^{\frac{q}{pq-1}}}{(pq-1)^{\frac{q+1}{pq-1}}}. \end{aligned} \tag{2.33}$$

Here, β_1 and β_2 satisfy

$$(p+1)\beta_1^{q+1} = (q+1)\beta_2^{p+1}. \tag{2.34}$$

To seek an approximate self-similar solution, we assume

$$f(y,s) = \beta_1\phi(\tfrac{y}{\alpha(s)}), \tag{2.35}$$

$$g(y,s) = \beta_2\psi(\tfrac{y}{\alpha(s)}), \tag{2.36}$$

$$z = \tfrac{y}{\alpha(s)}, \tag{2.37}$$

where β_1 and β_2 are affixed to ϕ and ψ to simplify future algebra. Substituting into (2.32), we have

$$\begin{aligned}\beta_1[(p+1)/(pq-1)\phi - z\phi_z\frac{\dot{\alpha}}{\alpha} + 1/2z\phi_z - \phi_{zz}\alpha^{-2}] = &\quad \beta_2^p\psi^p,\\ \beta_2[(q+1)/(pq-1)\psi - z\psi_z\frac{\dot{\alpha}}{\alpha} + 1/2z\psi_z - \psi_{zz}\alpha^{-2}] = &\quad \beta_1^q\phi^q.\end{aligned} \tag{2.38}$$

To keep consistent with the blowup nature of the solution, we assume further that

$$\begin{aligned}\alpha(s) &\to \infty \quad \text{as} \quad s \to \infty,\\ \frac{\dot{\alpha}(s)}{\alpha(s)} &\to 0, \quad \text{as} \quad s \to \infty,\end{aligned}$$

which implies that, near blowup time, (2.38) reduces to

$$\begin{aligned}\beta_1[(p+1)/(pq-1)\phi + 1/2z\phi_z] = &\quad \beta_2^p\psi^p,\\ \beta_2[(q+1)/(pq-1)\psi + 1/2z\psi_z] = &\quad \beta_1^q\phi^q.\end{aligned} \tag{2.39}$$

Substituting (2.33) into (2.39), we get

$$\begin{aligned}(p+1)/(pq-1)\phi + 1/2z\phi_z = &\quad \tfrac{p+1}{pq-1}\psi^p,\\ (q+1)/(pq-1)\psi + 1/2z\psi_z = &\quad \tfrac{q+1}{pq-1}\phi^q,\end{aligned} \tag{2.40}$$

whose solution is

$$\phi = \frac{1}{(1+cz^2)^{\frac{p+1}{pq-1}}}, \tag{2.41}$$

$$\psi = \frac{1}{(1+cz^2)^{\frac{q+1}{pq-1}}}, \tag{2.42}$$

where c is a constant depending on the initial conditions. Actually, there might be other solutions to (2.40), but our computational results suggest that, near blowup time,

$$(p+1)u^{q+1} = (q+1)v^{p+1}. \tag{2.43}$$

Substituting (2.29), (2.30), (2.35), (2.36) into (2.43) and using (2.33), we have

$$\phi^{q+1} = \psi^{p+1}. \tag{2.44}$$

The only solution of (2.40) that satisfies (2.44) is (2.41) and (2.42).

Consideration of higher order terms in (2.38) reveals that $\frac{\dot{\alpha}}{\alpha}$ and α^{-2} have the same order as s^{-1}, and we have (to the leading order)

$$\alpha(s) = As^{1/2}, \tag{2.45}$$

where A is a constant.

The monitor function, which, again, keeps (1.12) invariant under (2.28), can be

$$M = u^{(pq-1)/(p+1)}, \tag{2.46}$$

or

$$M = v^{(pq-1)/(q+1)},$$

or any linear combination of $u^{(pq-1)/(p+1)}$ and $v^{(pq-1)/(q+1)}$. We use the monitor function (2.46), which is used in our computations, to deduce the mesh behavior. Combining (2.41), (2.35) and (2.29), we have

$$u(x,t) = \beta_1(T-t)^{-\frac{p+1}{pq-1}}(1 + k\frac{(x-x^*)^2}{(T-t)|log(T-t)|})^{-\frac{p+1}{pq-1}} \tag{2.47}$$

where $k = \frac{c}{A^2}$. Substituting (2.47) into (2.46), we arrive at the following asymptotic form for M:

$$M = \beta_1^{-\frac{pq-1}{p+1}}(T-t)^{-1}(1 + k\frac{(x-x^*)^2}{(T-t)|log(T-t)|})^{-1}. \tag{2.48}$$

Integrating MMPDE6

$$\tau\frac{\partial^2\dot{x}}{\partial\xi^2} = -\frac{\partial}{\partial\xi}(M\frac{\partial x}{\partial\xi})$$

with respect to ξ, the mesh transformation $x(\xi,t)$ satisfies

$$-\tau\dot{x}_\xi = Mx_\xi + \theta(t). \tag{2.49}$$

Integrating again using the boundary conditions

$$x(0,t) = 0, \qquad x(1,t) = 1 \tag{2.50}$$

for the mesh transformation, we find

$$\theta(t) = -\int_0^1 M dx,$$

but for blowup solution $u(x,t)$, the integral is asymptotically dominated by the contribution from the blowup peak. Thus,

$$\theta(t) \approx -\int_{x^*-\epsilon}^{x^*+\epsilon} M\,dx.$$

The asymtotic formula (2.48) yields,

$$\begin{aligned}\theta(t) \approx & \quad -\beta_1^{\frac{pq-1}{p+1}}(T-t)^{-1}\int_{x^*-\epsilon}^{x^*+\epsilon}(1+k\tfrac{(x-x^*)^2}{(T-t)|log(T-t)|})^{-1}dx \\ = & \quad -\beta_1^{\frac{pq-1}{p+1}}(T-t)^{-\frac{1}{2}}|log(T-t)|^{\frac{1}{2}}\int_{-\epsilon(T-t)^{-\frac{1}{2}}|log(T-t)|^{-\frac{1}{2}}}^{\epsilon(T-t)^{-\frac{1}{2}}|log(T-t)|^{-\frac{1}{2}}}\tfrac{1}{1+ky^2}dy.\end{aligned}$$

As $t \to T$, the integral limits in the above integral tend to infinity; hence,

$$\begin{aligned}\theta(t) \approx & \quad -\beta_1^{\frac{pq-1}{p+1}}(T-t)^{-\frac{1}{2}}|log(T-t)|^{\frac{1}{2}}\int_{-\infty}^{+\infty}(1+ky^2)^{-1}dy, \\ = & \quad -\beta_1^{\frac{pq-1}{p+1}}(T-t)^{-\frac{1}{2}}|log(T-t)|^{\frac{1}{2}}\tfrac{\pi}{\sqrt{k}}. \qquad (2.51)\end{aligned}$$

From (2.31), (2.37), and (2.45), we know that

$$x(\xi,t) = x^* + (T-t)^{\frac{1}{2}}|log(T-t)|^{\frac{1}{2}}z(\xi). \qquad (2.52)$$

Substituting (2.48), (2.51), and (2.52) into (2.49), after some simplifications we have

$$\tau z_\xi(-\frac{1}{2}+\frac{1}{2}\frac{1}{|log(T-t)|}) = \beta_1^{\frac{pq-1}{p+1}}(1+kz^2)^{-1}z_\xi - \beta_1^{\frac{pq-1}{p+1}}\frac{\pi}{\sqrt{k}},$$

where the lefthand side is relatively very small if $\tau << 1$ and can be dropped. Therefore

$$(1+kz^2)^{-1}z_\xi = \frac{\pi}{\sqrt{k}},$$

and

$$z = \frac{\tan(\pi(\xi-\xi^*))}{\sqrt{k}}. \qquad (2.53)$$

Now (2.52), with boundary condition (2.50), implies that

$$z \to -\infty, \quad \text{as} \quad \xi \to 0; \quad z \to +\infty, \quad \text{as} \quad \xi \to 1.$$

This condition with (2.53) implies that

$$\xi^* = \frac{1}{2}.$$

So (2.52) becomes

$$x(\xi,t) = x^* + (T-t)^{\frac{1}{2}}|log(T-t)|^{\frac{1}{2}}\frac{\tan(\pi(\xi-\frac{1}{2}))}{\sqrt{k}}.$$

Substituting this into (2.47), we obtain

$$u(x,t) = \beta_1(T-t)^{-\frac{p+1}{pq-1}}[\cos(\pi(\xi-\frac{1}{2}))]^{\frac{2(p+1)}{pq-1}}. \tag{2.54}$$

Similarly,

$$v(x,t) = \beta_2(T-t)^{-\frac{q+1}{pq-1}}[\cos(\pi(\xi-\frac{1}{2}))]^{\frac{2(q+1)}{pq-1}}. \tag{2.55}$$

In conclusion, we conjecture from the formal analysis that the solution to (2.27) has the form (2.54) and (2.55). In the next subsection, we shall justify this form numerically.

2.2.2 Computational Results

In the following, all computations, starting with a uniform mesh, except where specified, are carried out with the following parameters: 41 mesh points, $atol = 1.d-8, rtol = 1.d-8$, $r = 1.d-5$, $ip = 1$. Also (2.46) is used with the moving mesh equation (1.12).

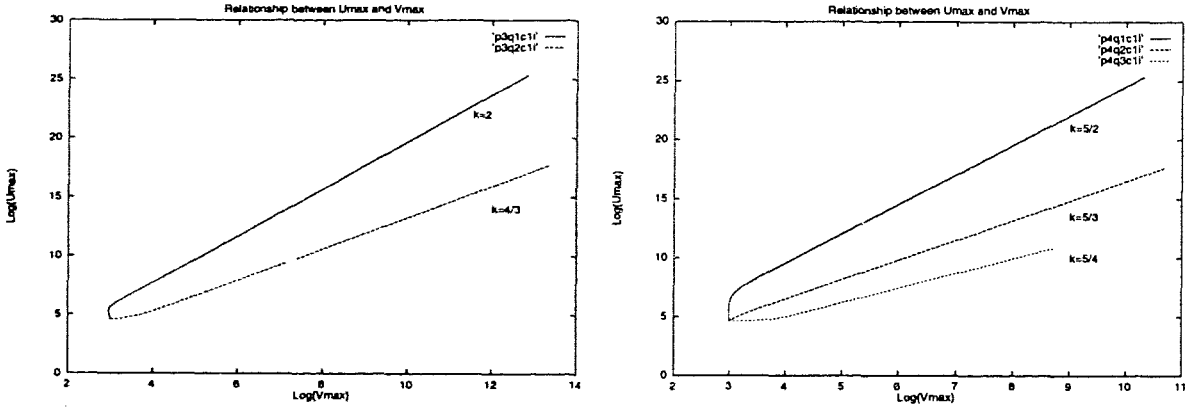

Figure 2.7: *For p=3, the slope is 2 and 4/3 respectively for q=1 and 2. For p=4, the slope is 5/2, 5/3, 5/4, respectively, for q=1, 2 and 3*

From (2.54) and (2.55), the formal analysis implies that

$$\begin{aligned} u_{max} &= \beta_1(T-t)^{-\frac{p+1}{pq-1}} \\ v_{max} &= \beta_2(T-t)^{-\frac{q+1}{pq-1}}, \end{aligned}$$

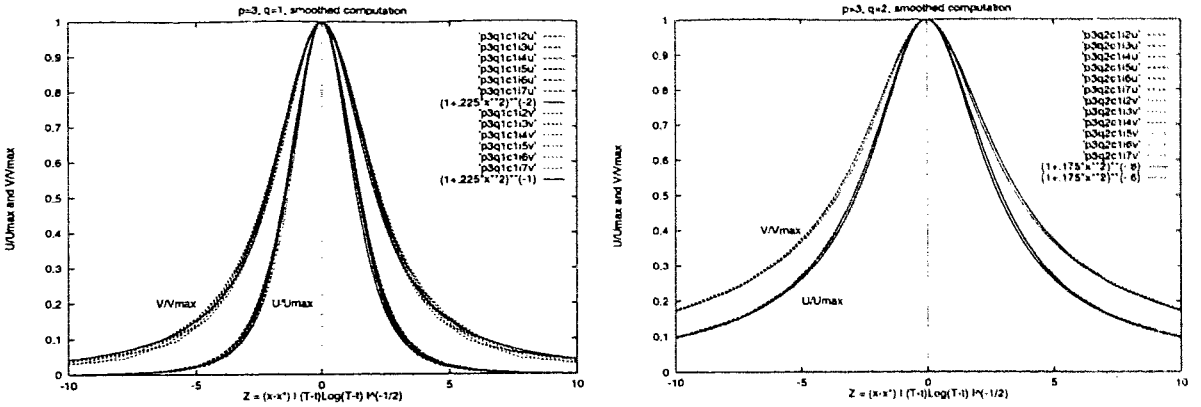

Figure 2.8: *Scaled solutions as functions of the ignitional kernel,p=3, q=2 and p=3, q=1*

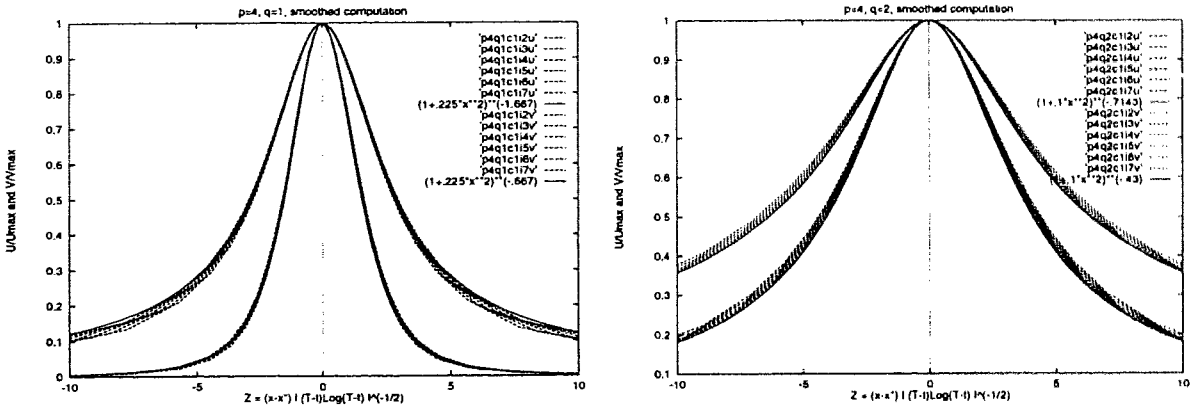

Figure 2.9: *Scaled solutions as functions of the ignitional kernel, p=4, q=1 and p=4, q=2*

which we confirm by plotting $\log(u_{max})$ as a function of $\log(v_{max})$. The function should be asymptotically a straight line with slope $\frac{p+1}{q+1}$. This is shown to be true in figure 2.7 for $p = 3$ and $p = 4$, respectively.

Also, (2.41) and (2.42) imply that asymptotically

$$\frac{u(x,t)}{u_{max}} = \phi(z) = (1+cz^2)^{-\frac{p+1}{pq-1}} \tag{2.56}$$

$$\frac{v(x,t)}{v_{max}} = \psi(z) = (1+cz^2)^{-\frac{q+1}{pq-1}} \tag{2.57}$$

where z is the ignitional kernel

$$z = (x-x^*)|(T-t)\log(T-t)|^{-\frac{1}{2}}.$$

This is demonstrated in figures 2.8, 2.9. In figure 2.8, $\frac{u}{u_{max}}$ and $\frac{v}{v_{max}}$ are approximately fixed functions of z, and two reference curves clearly show that $\phi = \psi^2$. In figure 2.9, we

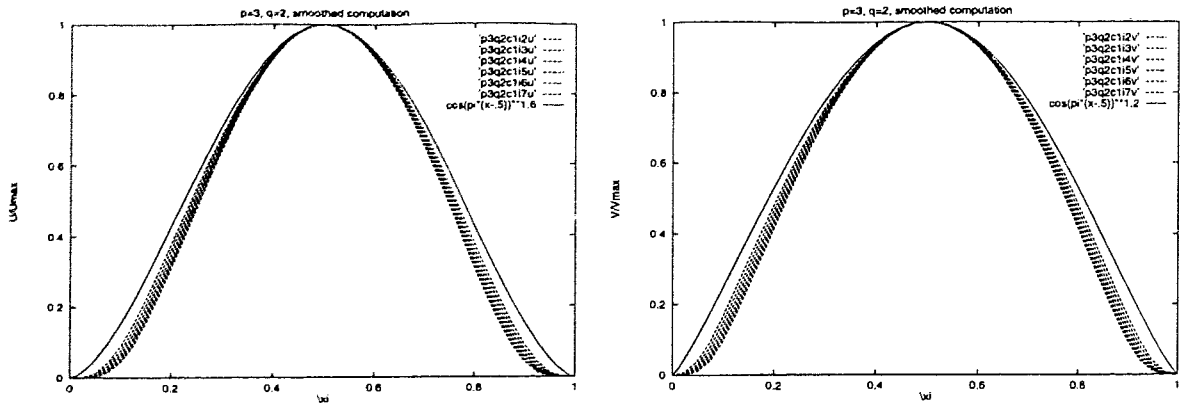

Figure 2.10: *Scaled solutions as functions of the computational coordinate,* $p = 3, q = 2$

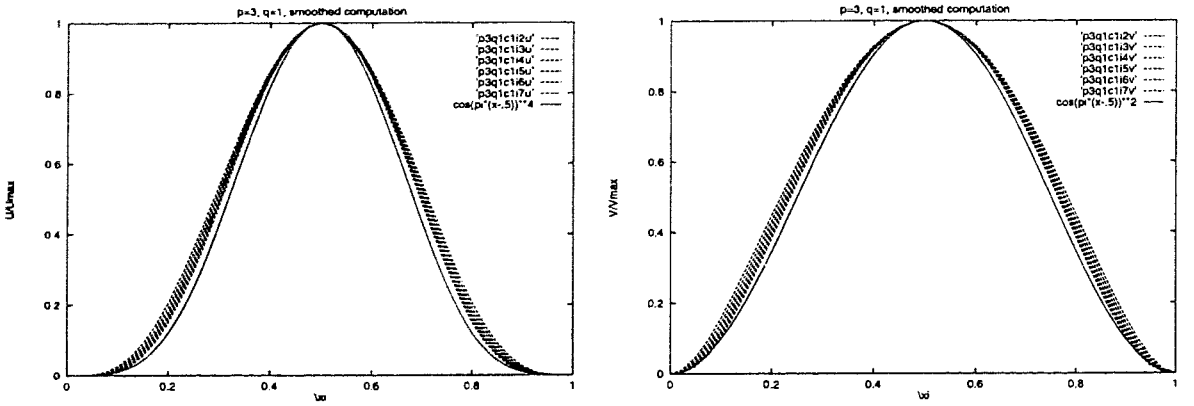

Figure 2.11: *Scaled solutions as functions of the computational coordinate,* $p = 3, q = 1$

demonstrate that (2.56) and (2.57) are true for other combinations of p and q. Actually, our computational results show that $(p+1)u^{q+1} = (q+1)v^{p+1}$.

Another result from (2.41) and (2.42) is that asymptotically

$$\frac{u(\xi,t)}{u_{max}} = [\cos(\pi(\xi - \frac{1}{2}))]^{\frac{2(p+1)}{pq-1}},$$
$$\frac{v(\xi,t)}{v_{max}} = [\cos(\pi(\xi - \frac{1}{2}))]^{\frac{2(q+1)}{pq-1}}.$$

This is shown to be true in figures 2.10, 2.11 for some combinations of p and q.

During the computations, we also observed that the physical blowup point may change in accordance with the relative magnitude and local structure of the initial conditions. But a discussion of the relationship between the blowup point and the initial conditions is beyond the scope of this study.

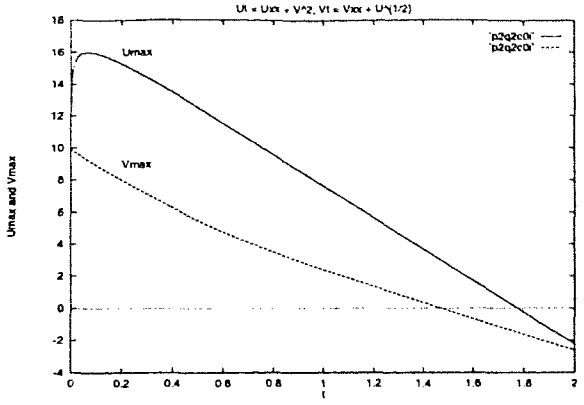

Figure 2.12: *A decaying solution*

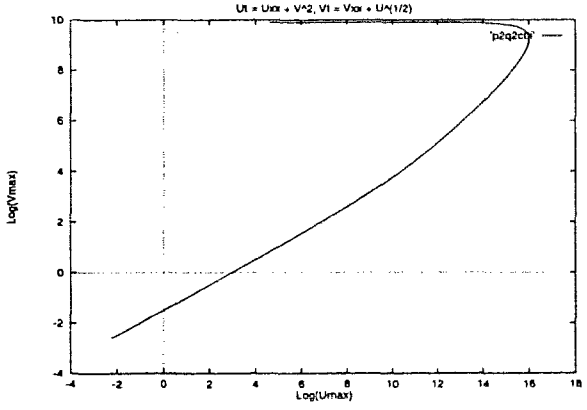

Figure 2.13: *Relationship between* $u_{\max}$ *and* $v_{\max}$ *while decaying*

In [15], it has been also shown that if $pq \leq 1$, then the solution is global, i.e., no blowup occurs. When we tried some computations with $pq = 1$, even with large initial conditions the solution decayed, as shown in figures 2.12 and 2.13 for $p = 2, q = 1/2$. The initial condition used here is $u_0(x) = 100\sin(\pi x), v_0(x) = 20000\sin(\pi x)$. For other combinations of p and q with $pq \leq 1$, similar results are obtained.

It is interesting to observe that if $pq > 1$ but $(\gamma + 1)/(pq - 1) < 1/2$ (in the one dimensional case) with $\gamma = \max\{p, q\}$, the solution behaviour is mixed (as predicted in [15]). For $p = 4, q = 3$, with initial condition $u_0(x) = 4.75\sin(\pi x), v_0(x) = .9\sin(\pi x)$, a blowup solution with magnitude $u_{\max} = 5 \times 10^4$ is observed while with initial condition $u_0(x) = 4.5\sin(\pi x), v_0(x) = .9\sin(\pi x)$ the solution decayed.

The above results demonstrate that our method not only can compute the blowup solutions accurately but can also *automatically* distinguish between blowup and non-blowup

solutions.

2.3 Blowup in a Set

In this section, we consider the initial value problem

$$u_t = (u^\sigma u_x)_x + u^{\sigma+1}, \quad \text{for } x \in (-\infty, +\infty), \quad t > 0, \tag{2.58}$$

with

$$u(x,0) = u_0(x), \quad x \in R^1, \tag{2.59}$$

where $\sigma > 0$ is a constant.

Assume the initial condition (2.59) satisfies

$$\begin{aligned} &u_0(x) \geq 0, u_0 \not\equiv 0 \text{ in } R^1; M_1 = \sup u_0 < +\infty; \\ &u_0^\sigma(x) \text{ is uniformly Lipschitz continuous in } R^1; \\ &\text{supp } u_0(x) \equiv \{x \in R^1 | u_0(x) > 0\} \text{ is a bounded set,} \end{aligned} \tag{2.60}$$

where M_1 and M_2 are positive constants.

It is well known ([19] and references therein) that, under the above hypotheses, the Cauchy problem (2.58),(2.59) has a unique local (in time) weak solution $u(x,t)$ which is a nonnegative continuous function. Since $u_0 \not\equiv 0$, this solution blows up in finite time [20].

The blow-up set is defined as

$$\begin{aligned} B = B(u_0) \equiv \{ \quad & x \in R^1 | \text{ there exists } x_n \to x \text{ and } t_n \to T_0 \\ & \text{such that } u(x_n, t_n) \to +\infty \text{ as } n \to \infty\}. \end{aligned}$$

Equation (2.58) is invariant under the self-similar transformation

$$\begin{aligned} T - \bar{t} = &\quad \lambda(T-t), \\ \bar{x} - x^* = &\quad x - x^*, \\ \bar{u} = &\quad \lambda^{-\frac{1}{\sigma}} u. \end{aligned} \tag{2.61}$$

It has been shown [19] that assuming the blowup set is centered at 0, i.e. $x^* = 0$, equation (2.58) admits the (blow-up) self-similar weak solution

$$u_s(x,t) = (T_0 - t)^{-\frac{1}{\sigma}} \theta_s(x) \tag{2.62}$$

where

$$\theta_s(x) = \left[\frac{2(\sigma+1)}{\sigma(\sigma+2)}\cos^2(\frac{\pi x}{L_s})\right]^{\frac{1}{\sigma}}, \quad \text{for} \quad |x| \le \frac{L_s}{2}$$
$$\theta_s(x) = 0, \quad \text{for} \quad |x| \ge \frac{L_s}{2}. \tag{2.63}$$

Here

$$L_s = \frac{2\pi(\sigma+1)^{\frac{1}{2}}}{\sigma}$$

is the so-called fundamental length.

In the numerical computations which are described below, we change the Cauchy problem (2.58) into an initial-boundary value problem with boundary condition

$$u(L,t) = 0, \quad u(R,t) = 0$$

where L and R are the left and right end of an interval in which (2.59) is defined. Actually, in the following computations, we choose $L = -5$ and $R = 5$.

As a monitor function, we take

$$M = u^\sigma,$$

which makes the MMPDE6 (1.12) invariant under the transformation (2.61).

From (2.63), we know that the blowup set is

$$B = [-\frac{L_s}{2}, \frac{L_s}{2}] \tag{2.64}$$

which is independent of the initial condition as long as (2.60) is satisfied.

In figure 2.14, we present a solution with magnitude $u_{\max} = 1.0 \times 10^5$ computed for $\sigma = 2$ using (1.12) as the moving mesh equation, with the following parameters: $N = 41$, $atol = 10^{-8}, rtol = 10^{-10}$, $\tau = 10^{-5}$. In the figure, the curve "S1" stands for the solution obtained with the initial condition $u_0(x) = 0.01(5-x)^2(5+x)^2$ (which is the curve "I1" in the figure), whose support contains the blowup set. The solution "S2" is obtained with the initial condition $u_0(x) = 10(1-x)^2(1+x)^2$ (the curve "I2" in the figure) whose support is contained in the blowup set. As shown in the figure, both solution profiles match the solution $\cos(\frac{x}{\sqrt{3}})$ predicted by (2.63) for $\sigma = 2$, and the blowup set obtained matches that given in (2.64).

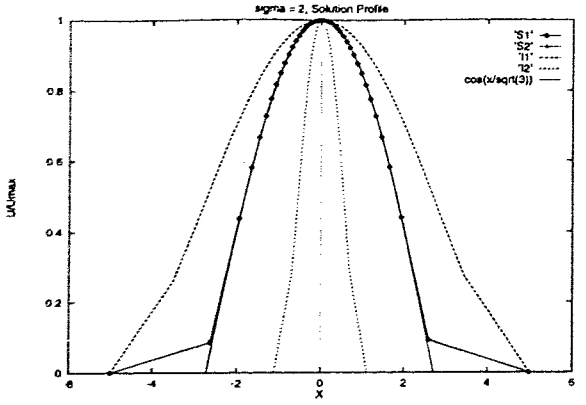

Figure 2.14: *Blowup in a set: solution profile*

From (2.62) and (2.63), we know that

$$u_{\max}^{-\sigma} = (T-t)\left(\frac{2(\sigma+1)}{\sigma(\sigma+2)}\right)^{-1},$$

i.e., $u_{\max}^{-\sigma}$ is a linear function of t near blowup time with the slope $-(\frac{2(\sigma+1)}{\sigma(\sigma+2)})^{-1}$. For $\sigma = 2$, the slope is $-4/3 \approx -1.333$. This is shown to be approximately true in figure 2.15 for computations with four different initial conditions.

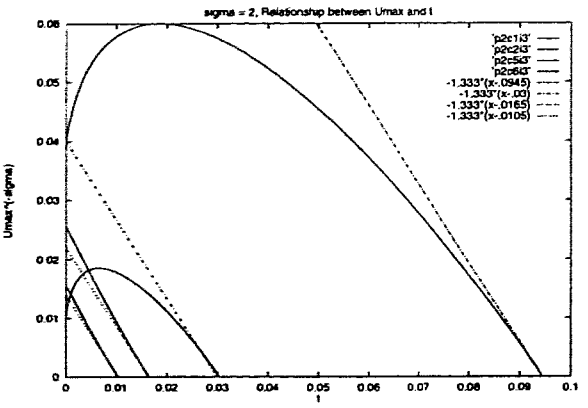

Figure 2.15: *Blowup in a set: magnitude*

For other σ values, similar results can be obtained with properly chosen parameters.

2.4 Summary

The moving mesh method has been shown to be successful [10] in computing the solution for blowup problems. In this chapter, this method is used on several blowup problems.

In section 2.1, we studied a degenerate blowup problem. Compared with the asymptotic analysis, our method gives accurate prediction of spatial blowup features, especially the blowup point and the blowup time. In principle, our method can be used to study the delicate relationship between the initial conditions and the blowup time and point.

We study a blowup system in section 2.2. With the help of the numerical computations, we completed a formal analysis for the system. The insight gained from the computations plays an important role in the analysis. We also demonstrate that our method automatically distinguishes between blowup and nonblowup solutions, making it reliable for studying other problems with possible blowup solutions. To the author's knowledge, this is the first extensive numerical study and asymptotic analysis for such systems.

Another challenging problem for numerical computation, heat conduction with temperature dependent conductivity and nonlinear forcing, is studied in section 2.3. This problem evidently has blowup in a set, and the computed blowup set matches with that predicted by asymptotic analysis.

Chapter 3

Moving Mesh Method and Conservation Laws

In this chapter, we consider the scalar conservation law

$$u_t + (f(u))_x = 0. \tag{3.1}$$

There is an extensive literature concerning numerical methods for (3.1), however adaptive approaches seem to be underrepresented. A recent study of adaptive methods for solving (3.1) is by Bell [7]. He used a static mesh refinement method based on a sequence of nested locally uniform grids. His method depends on local error estimation and the efficiency of his method is problem dependent. Biswas and co-workers [8] studied (3.1) with a hybrid of moving mesh and local refinement methods. Their emphasis is on the local mesh refinement, their global mesh motion does not always work well, and incorrect mesh movement may occur. A static mesh regridding method was studied by Lucier [35]. Harten and Hyman studied (3.1) with a self-adjusting mesh [23]. Actually, Harten and Hyman's approach is to compute the solution on a *fixed* mesh by adjusting the ends of the intervals on which the computed solution is a piecewise constant approximation to the exact solution. Their schemes do not perform very well in rarefaction regions, and in some cases noticeable non-physical oscillations can be observed. In this chapter, we study (3.1) with our moving mesh methods. The motivation is to study the sensitivity of the computations to the spatial discretizations and find out how adaptive viscosity is provided by the moving mesh methods. The moving mesh method has previously been shown to be successful for conservation laws with artificial viscosity term [29], [44], [45]. But the artificial viscosity term smears

the solution, and the difficulties of computing possibly discontinuous weak solutions are not overcome but avoided. The purpose here is to investigate the possibility of designing a moving mesh equation for inviscid conservation laws.

In section 3.1, we compare the computations on a fixed mesh with those on an adaptive mesh to uncover the mechanism that keeps moving mesh computations stable. In section 3.2, a new Godunov type adaptive method of lines approach to conservation laws is developed, and some computational results are shown to demonstrate the performance of this new method.

3.1 A Finite Difference Approach

In this section, we study the method of lines approach for conservation laws with artificial viscosity term on both a fixed mesh and a moving mesh.

In the first chapter, we have shown that adaptive methods are based on the coordinate transformation $(x,t) \rightarrow (\xi,t)$. After this transformation, a conservation law with artificial viscosity term,

$$u_t + (f(u))_x = \epsilon u_{xx}, \tag{3.2}$$

becomes

$$\dot{u} - u_x\dot{x} + (f(u))_x = \epsilon u_{xx}. \tag{3.3}$$

Several spatial discretizations can be used to approximate the first order spatial derivatives in (3.3). We use the following two to make our comparisons.

1. (3-point) Centered finite differences:

$$(f_x)_j \approx \frac{f_{j+1} - f_{j-1}}{x_{j+1} - x_{j-1}},$$

where $f_j := f(u_j)$. The truncation error is

$$-\frac{f''(u_j)}{2} \cdot ((x_{j+1} - x_j) - (x_j - x_{j-1}))$$
$$-\frac{f'''(u_j)}{6}\left[(x_{j+1} - x_j)^2 - (x_{j+1} - x_j)(x_j - x_{j-1}) + (x_j - x_{j-1})^2\right],$$

which is of the magnitude of the larger one of $x_{j+1} - x_j$ and $x_j - x_{j-1}$ if one is much larger than the other.

2. (3-point) Varied centered finite differences:

$$(f_x)_j \approx \frac{1}{x_{j+1}-x_{j-1}}\left(\frac{f_{j+1}-f_j}{x_{j+1}-x_j}\cdot(x_j-x_{j-1})+\frac{f_j-f_{j-1}}{x_j-x_{j-1}}\cdot(x_{j+1}-x_j)\right) \tag{3.4}$$

Using the Taylor's expansions

$$f'(x)=\frac{f(x+\Delta x_1)-f(x)}{\Delta x_1}-\frac{f''(x)}{2}\Delta x_1+O(\Delta x_1^2), \tag{3.5}$$

$$f'(x)=\frac{f(x)-f(x-\Delta x_2)}{\Delta x_2}+\frac{f''(x)}{2}\Delta x_2+O(\Delta x_2^2), \tag{3.6}$$

where $\Delta x_1 := x_{j+1}-x_j$ and $\Delta x_2 := x_j - x_{j-1}$, adding (3.5) times Δx_2 and (3.6) times Δx_1, we obtain (3.4) with a local truncation error

$$-\frac{f'''(u_j)}{6}(x_{j+1}-x_j)(x_j-x_{j-1}). \tag{3.7}$$

This scheme will reduce to the standard centered finite difference on a uniform mesh.

The u_{xx} term in (3.3) is approximated by

$$(u_{xx})_j \approx \frac{2}{x_{j+1}-x_{j-1}}\left(\frac{u_{j+1}-u_j}{x_{j+1}-x_j}-\frac{u_j-u_{j-1}}{x_j-x_{j-1}}\right),$$

whose truncation error is

$$\frac{(u_{xxx})_j}{3}\left((x_{j+1}-x_j)(x_j-x_{j-1})\right).$$

In the computations which follow we specify our flux function $f(u)=\frac{u^2}{2}$, that is, we use inviscid Burgers' equation:

$$u_t+\left(\frac{u^2}{2}\right)_x=0, \tag{3.8}$$

as our basis problem for numerical experiments.

We first test our spatial discretizations on a uniform mesh for viscous Burgers' equation:

$$u_t+\left(\frac{u^2}{2}\right)_x=\epsilon u_{xx}, \tag{3.9}$$

with the initial and boundary conditions

$$\begin{aligned} u(x,0) &= \sin(2\pi x)+\frac{1}{2}\sin(\pi x), \quad 0\le x\le 1,\\ u(0,t) &= u(1,t)=0, \quad t>0. \end{aligned}$$

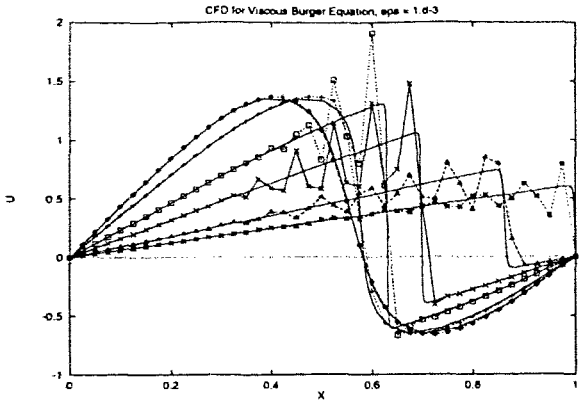

Figure 3.1: $\epsilon = 1.d-3$ *with fixed uniform mesh*

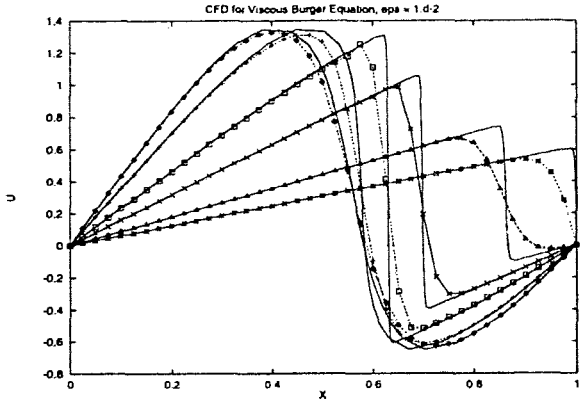

Figure 3.2: $\epsilon = 1.d-2$ *with fixed uniform mesh*

In the computations, we used 40 *fixed* uniform mesh points and absolute and relative error tolerance $atol = rtol = 1.d-6$ for DDASSL. In this case, varied centered finite differences is identical to centered finite differences.

Two results are presented in figures 3.1 and 3.2 for computations with centered finite differences for both u_x and $(f(u))_x$ terms in (3.3) with $\epsilon = 1.d-3$ and $\epsilon = 1.d-2$, respectively. In the figures, solid lines denote the reference solutions obtained by coupling (3.9) with MMPDE4 (1.10) with parameters $\tau = 1.d-5$, $ip = 1$, $rtol = atol = 1.d-6$, $\epsilon = 10^{-3}$ and arclength monitor function $M = \sqrt{1+u_x^2}$.

There are two things worth noting here:

1. In the computation with $\epsilon = 1.d-3$, large oscillations in the solution are observed while with $\epsilon = 1.d-2$ the solution is oversmoothed. This phenomena clearly shows the dilemma with artificial viscosity: it is difficult to determine the appropriate amount for

the artificial viscosity that introduces just enough dissipation to preserve monotonicity without causing unnecessary smearing.

2. Recall that, with proper moving mesh methods, the computation with centered finite differences is successful with similar parameters [29] while a fixed mesh fails, we can conjecture that some *adaptive* viscosity was introduced by the moving mesh equation. In other words, one important function of the moving mesh methods is to introduce viscosity *adaptively.*

Now, we turn our attention to the moving mesh method for conservation laws. With the above observation in hand, assuming the moving mesh equation can be solved exactly, we can undo the change of variables introduced and transform (3.3) back to (3.2), and no additional terms are introduced. This reveals that no adaptive viscosity will be produced by the first two terms in (3.3) independent of the moving mesh equation chosen, or adaptive viscosity comes from spatial discretization of the derivatives in (3.3).

Now, let us consider the discretization of (3.3). If a centered finite difference is used in (3.3), we obtain

$$\dot{u}_i - \frac{u_{i+1}-u_{i-1}}{x_{i+1}-x_{i-1}}\dot{x}_i + \frac{f_{i+1}-f_{i-1}}{x_{i+1}-x_{i-1}} = \epsilon \frac{2}{x_{i+1}-x_{i-1}}\left(\frac{u_{i+1}-u_i}{x_{i+1}-x_i} - \frac{u_i-u_{i-1}}{x_i-x_{i-1}}\right). \tag{3.10}$$

The leading term of the truncation error in (3.10) is

$$\begin{aligned} &\dot{x}_i \frac{(u_{xx})_i}{2}((x_{i+1}-x_i)-(x_i-x_{i-1})) \\ -&\frac{((f(u))_{xx})_i}{2}((x_{i+1}-x_i)-(x_i-x_{i-1})) \\ &+\epsilon\frac{u_{xxx}}{3}((x_{i+1}-x_i)-(x_i-x_{i-1})) \end{aligned}$$

where $((x_{i+1}-x_i)-(x_i-x_{i-1}))$ can be regarded as a second order approximation to $\Delta\xi^2\frac{\partial^2 x}{\partial \xi^2}$. Therefore, the solution obtained by (3.10) is actually, to a higher order of approximation, the solution of:

$$\dot{u} - u_x\dot{x} + (f(u))_x = \epsilon u_{xx} - \frac{\Delta\xi^2}{2}\frac{\partial^2 x}{\partial \xi^2}\dot{x}u_{xx} + \frac{\Delta\xi^2}{2}\frac{\partial^2 x}{\partial \xi^2}(f(u))_{xx} + \epsilon\frac{\Delta\xi^2}{3}\frac{\partial^2 x}{\partial \xi^2}u_{xxx}. \tag{3.11}$$

It is clear from (3.11) that the adaptive viscosity of moving mesh methods comes in from the numerical viscosity, the second derivative terms in (3.11). With centered finite difference discretization for (3.2) the conservation law with artificial viscosity term, the moving mesh

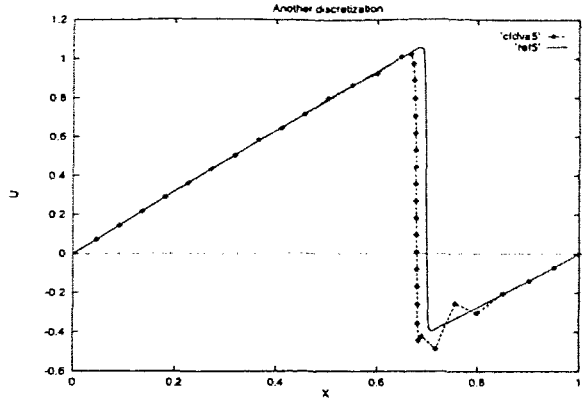

Figure 3.3: *Varied centered finite difference for* u_x, $\epsilon = 10^{-3}$

method is implicitly an adaptive viscosity method. The adaptivity depends heavily on the mesh distribution ($\frac{\partial^2 x}{\partial \xi^2}$). Thus, a carefully chosen monitor function and moving mesh equation will be essential to the success of the moving mesh methods.

A varied centered finite difference (3.4) for u_x (but centered finite difference for $f(u)_x$) eliminates the second term and introduces another dispersive term $-\frac{\Delta\xi^2}{6}\left(\frac{\partial x}{\partial \xi}\right)^2 \dot{x} u_{xxx}$ on the right hand in (3.11). A computational result using MMPDE6 (1.12) as the moving mesh equation, arclength monitor function, and $\epsilon = 10^{-3}$, is shown in figure 3.3 with time $t = 0.3$ (other parameters are the same as before). Compared with the reference solution, the solid line in the figure, the shock falls far behind and some oscillations are observed. The presence of oscillations indicates that the viscosity is insufficient to damp the artificial dispersion (the last term in (3.11)). Similarly, a varied centered finite difference for $(f(u))_x$ eliminates the

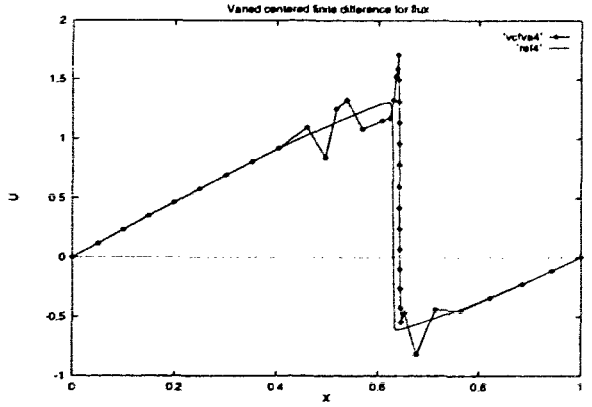

Figure 3.4: *Varied centered finite difference for* $f(u)_x$, $\epsilon = 10^{-3}$

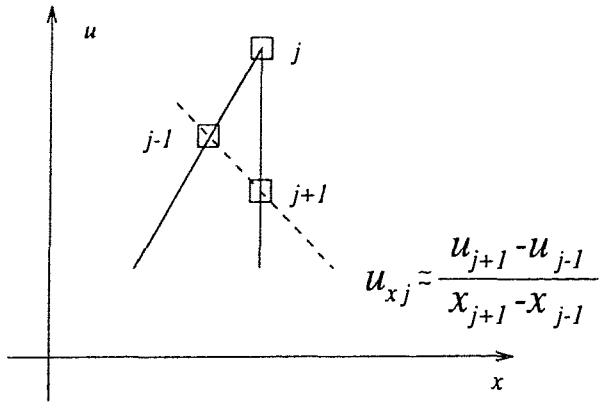

Figure 3.5: *Numerical approximation of* u_{xj}

third term and introduces another term $-\frac{\Delta\xi^2}{6}\left(\frac{\partial x}{\partial \xi}\right)^2 f_{xxx}$ on the right hand side in (3.11). Computational result shows a shock faster than the reference solution with large oscillations (see figure 3.4).

Notice that at the corner point where u_{xx} and $\frac{\partial^2 x}{\partial \xi^2}$ are relatively large (compared with smooth region), numerically $u_x^2 \ll u_{xx}$ (see figure 3.5), $\epsilon u_{xxx} \ll u_{xx}$,

$$\begin{aligned}(f(u))_{xx} &= f_{uu} \cdot u_x^2 + f_u \cdot u_{xx} \\ &\approx f_u \cdot u_{xx}.\end{aligned}$$

Under this approximation the right hand side of (3.11) reduces to

$$\epsilon u_{xx} + \frac{\Delta\xi^2}{2}\frac{\partial^2 x}{\partial \xi^2}(f_u - \dot{x})u_{xx}, \tag{3.12}$$

which implies that if the mesh speed is drifting away from the characteristic speed f_u, some viscosity is added at the corner points. It is not yet clear whether this property may lead to an entropy condition (which guarantees the computed solution is the physical solution [33]) as $\epsilon \to 0$. The above varied centered finite difference discretizations apparently lack an entropy condition as evidenced by the computed shock speed drifting away from the physical speed and the generation of the oscillations.

Now, let us consider the effect of decreasing ϵ on the efficiency of the moving mesh methods with centered finite difference discretization. Typical integration behavior for different ϵ's (with MMPDE6 (1.12) as moving mesh equation, arclength monitor function $M = \sqrt{1 + u_x^2}$, and $\tau = 10^{-5}$) are listed in table 3.1. It shows that min $\Delta x \sim \epsilon$ and $\Delta t \sim \epsilon$.

ϵ	$\min \Delta x$	Δt
10^{-3}	0.2×10^{-3}	0.5×10^{-3}
10^{-4}	0.2×10^{-4}	0.2×10^{-4}
10^{-5}	0.25×10^{-5}	0.5×10^{-5}
10^{-6}	0.5×10^{-6}	0.1×10^{-6}

Table 3.1: *Comparison of temporal and spatial steps with different* ϵ

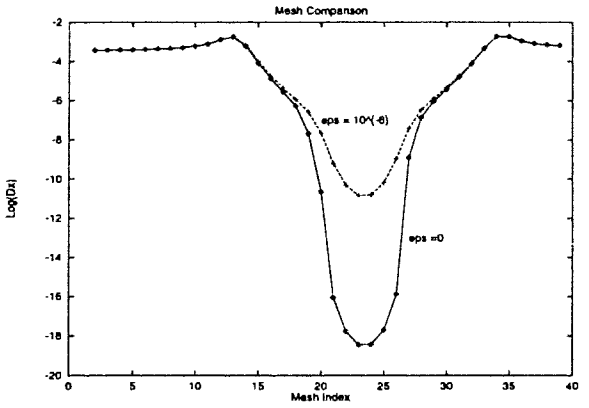

Figure 3.6: *Mesh behavior of inviscid conservation law and* $\epsilon = 10^{-6}$

Not surprisingly, the computation without the artificial viscosity term ϵu_{xx} or $\epsilon = 0$ collapses. In figure 3.6, we plot $\log(\Delta x)$, where $\Delta x_i = x_i - x_{i-1}$, at different mesh points for computations with (1.12) as moving mesh equation and $\tau = 10^{-3}$ before the time step reaches 10^{-9}. An examination of the mesh distribution plot reveals that the mesh distribution becomes too far away from uniform mesh with $\Delta x_i \ll \Delta x_{i+1}$ at some points, which greatly complicates the above analysis and necessitates the inclusion of higher order terms.

In summary, the finite difference approach to the conservation laws requires artificial viscosity to keep the computation stable. When ϵ becomes very small, the method becomes inefficient. Noticing that, with the arclength monitor function, many mesh points are located in the shock region (so called over-resolved shock) with $\min \Delta x \sim \epsilon$, the resolution to the shock is smeared. Proper spatial discretization is required to obtain a nonoscillatory physically correct weak solution.

3.2 A Godunov Type Approach

In this section, we consider conservation laws without artificial viscosity (3.1). First of all, we derive an ODE for the cell average of the solution for conservation law (3.1) in an adaptive environment based on a Godunov type approach.

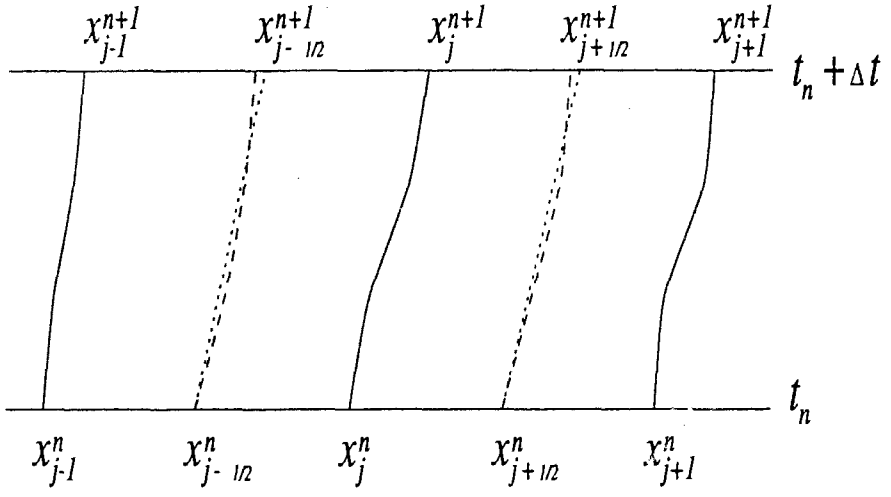

Figure 3.7: *Goduniv type schemes in an adaptive envirment*

Considering the adaptive mesh shown in figure 3.7, we consider our computed solution $\bar{U}_j^n$ as the average of the exact solution $u(x,t)$ over $[x_{j-\frac{1}{2}}^n, x_{j+\frac{1}{2}}^n]$ at time t_n, and define $\tilde{u}(x,t)$ as the exact solution for the conservation law with pointwise function $\tilde{U}(x)$ (which is either piecewise constant or piecewise linear with cell average $\bar{U}_j^n$) as the initial condition for $t_n < t < t_n + \Delta t$, where Δt is a small time step. Taking an approach similar to that used by Godunov [33], we notice that, for piecewise constant $\tilde{U}(x)$, the exact solution $\tilde{u}(x,t), t_n < t < t_n + \Delta t$ can be obtained by solving a sequence of Riemann problems and piecing together these Riemann solutions. For piecewise linear $\tilde{U}(x)$, $\tilde{u}(x,t)$ can be obtained by solving the conservation law (3.1) with a piecewise linear initial data. If we define $U_j(t)$ as the cell average of $\tilde{u}(x,t)$ for $t_n < t < t_n + \Delta t$, we have

$$U_j(t) := \frac{\int_{x_{j-\frac{1}{2}}(t)}^{x_{j+\frac{1}{2}}(t)} \tilde{u}(x,t)dx}{x_{j+\frac{1}{2}}(t) - x_{j-\frac{1}{2}}(t)}, \qquad t_n < t < t_n + \Delta t. \tag{3.13}$$

Differentiating (3.13) with respect to t, we have

$$\begin{aligned}\dot{U}_j(t) := \frac{dU_j}{dt} &= \frac{\frac{d}{dt}\int_{x_{j-\frac{1}{2}}(t)}^{x_{j+\frac{1}{2}}(t)} \tilde{u}(x,t)dx}{x_{j+\frac{1}{2}}(t) - x_{j-\frac{1}{2}}(t)} - \frac{\int_{x_{j-\frac{1}{2}}(t)}^{x_{j+\frac{1}{2}}(t)} \tilde{u}(x,t)dx \cdot \left(\dot{x}_{j+\frac{1}{2}}(t) - \dot{x}_{j-\frac{1}{2}}(t)\right)}{\left(x_{j+\frac{1}{2}}(t) - x_{j-\frac{1}{2}}(t)\right)^2}, \\ &= \frac{\int_{x_{j-\frac{1}{2}}(t)}^{x_{j+\frac{1}{2}}(t)} \frac{\partial \tilde{u}(x,t)}{\partial t}dx + \tilde{u}(x_{j+\frac{1}{2}},t)\cdot\dot{x}_{j+\frac{1}{2}}(t) - \tilde{u}(x_{j-\frac{1}{2}},t)\cdot\dot{x}_{j-\frac{1}{2}}(t)}{x_{j+\frac{1}{2}}(t) - x_{j-\frac{1}{2}}(t)} \\ &\quad - \frac{\int_{x_{j-\frac{1}{2}}(t)}^{x_{j+\frac{1}{2}}(t)} \tilde{u}(x,t)dx \cdot \left(\dot{x}_{j+\frac{1}{2}}(t) - \dot{x}_{j-\frac{1}{2}}(t)\right)}{\left(x_{j+\frac{1}{2}}(t) - x_{j-\frac{1}{2}}(t)\right)^2}.\end{aligned}$$

Since $\tilde{u}(x,t)$ is the exact solution, we can use (3.1) and (3.13) to obtain

$$\begin{aligned}\dot{U}_j(t) &= \frac{-\int_{x_{j-\frac{1}{2}}(t)}^{x_{j+\frac{1}{2}}(t)} [f(\tilde{u}(x,t))]_x dx + \tilde{u}(x_{j+\frac{1}{2}},t)\cdot\dot{x}_{j+\frac{1}{2}}(t) - \tilde{u}(x_{j-\frac{1}{2}},t)\cdot\dot{x}_{j-\frac{1}{2}}(t)}{x_{j+\frac{1}{2}}(t) - x_{j-\frac{1}{2}}(t)} \\ &\quad - \frac{U_j(t)\cdot\left(\dot{x}_{j+\frac{1}{2}}(t) - \dot{x}_{j-\frac{1}{2}}(t)\right)}{x_{j+\frac{1}{2}}(t) - x_{j-\frac{1}{2}}(t)}, \\ &= \frac{-f(\tilde{u}(x_{j+\frac{1}{2}},t)) + f(\tilde{u}(x_{j-\frac{1}{2}},t)) + \tilde{u}(x_{j+\frac{1}{2}},t)\cdot\dot{x}_{j+\frac{1}{2}}(t) - \tilde{u}(x_{j-\frac{1}{2}},t)\cdot\dot{x}_{j-\frac{1}{2}}(t)}{x_{j+\frac{1}{2}}(t) - x_{j-\frac{1}{2}}(t)} \\ &\quad - \frac{U_j(t)\cdot\left(\dot{x}_{j+\frac{1}{2}}(t) - \dot{x}_{j-\frac{1}{2}}(t)\right)}{x_{j+\frac{1}{2}}(t) - x_{j-\frac{1}{2}}(t)};\end{aligned}$$

therefore, the ODE for $U_j(t)$ in conservative form is

$$\begin{aligned}\dot{U}_j &= -\frac{\left[f(\tilde{u}(x_{j+\frac{1}{2}},t)) + U_j(t)\cdot\dot{x}_{j+\frac{1}{2}}(t)\right] - \left[f(\tilde{u}(x_{j-\frac{1}{2}},t)) + U_j(t)\cdot\dot{x}_{j-\frac{1}{2}}(t)\right]}{x_{j+\frac{1}{2}}(t) - x_{j-\frac{1}{2}}(t)} \\ &\quad + \frac{\tilde{u}(x_{j+\frac{1}{2}},t)\cdot\dot{x}_{j+\frac{1}{2}}(t) - \tilde{u}(x_{j-\frac{1}{2}},t)\cdot\dot{x}_{j-\frac{1}{2}}(t)}{x_{j+\frac{1}{2}}(t) - x_{j-\frac{1}{2}}(t)},\end{aligned} \tag{3.14}$$

where the quantity $f(\tilde{u}(x_{j\pm\frac{1}{2}},t)) + U_j(t)\cdot\dot{x}_{j\pm\frac{1}{2}}(t)$ plays the role of the flux function. A similar flux function was used by Harten and Hyman in [23]. Assuming the existence of

$\tilde{u}(x,t)$, the above derivation is independent of the definition of the initial pointwise function $\tilde{U}(x)$. The same derivation carries through for a system of conservation laws in one space dimension without any modification.

Now, we define our adaptive Godunov type schemes.

1. adaptive Godunov scheme:

   Definiting $\tilde{U}(x) = \bar{U}_j^n, x \in [x_{j-\frac{1}{2}}^n, x_{j+\frac{1}{2}}^n]$, i.e. reconstructing the solution at $t = t_n$ in a piecewise *constant* fashion, $\tilde{u}(x,t)$ can be obtained by solving a sequence of Riemann problems and piecing together the solutions. Noticing that $x_{j+\frac{1}{2}}(t) \approx x_{j+\frac{1}{2}}^n + t\dot{x}_{j+\frac{1}{2}}(t_n + \Delta t), t_n < t < t_n + \Delta t$ and $\tilde{u}(x,t)$ is a constant along the line $x(t) = x_{j+\frac{1}{2}}^n + t\dot{x}_{j+\frac{1}{2}}(t_n + \Delta t), t_n < t < t_n + \Delta t$ if no interaction occurs between neighbouring Riemann problems, we can reasonably approximate $\tilde{u}\left(x_{j+\frac{1}{2}}(t), t\right)$ in (3.14) by that constant. Thus, $\tilde{u}\left(x_{j+\frac{1}{2}}(t), t\right)$ in (3.14) can be approximated with $u^*\left(\dot{x}_{j+\frac{1}{2}}(t); \bar{U}_j^n, \bar{U}_{j+1}^n\right)$ where $u^*(x/t; u_l, u_r)$ is the solution of the Riemann problem

$$u_t + f(u)_x = 0, \tag{3.15}$$
$$u(x,0) = \begin{cases} u_l, & \text{if } x < 0, \\ u_r, & \text{if } x > 0. \end{cases}$$

   We call this first order scheme an adaptive Godunov scheme.

2. adaptive Osher scheme:

   We can also reconstruct the solution at $t = t_n$ in a piecewise *linear* fashion, i.e., $\tilde{U}(x) = \bar{U}_j^n + \sigma_j(x - x_j^n), x \in [x_{j-\frac{1}{2}}^n, x_{j+\frac{1}{2}}^n]$, where σ_j is the slope limiter defined by

$$\sigma_j = \text{minmod}\left(\frac{\bar{U}_{j+1}^n - \bar{U}_j^n}{x_{j+1}^n - x_j^n}, \frac{\bar{U}_j^n - \bar{U}_{j-1}^n}{x_j^n - x_{j-1}^n}\right)$$

   and the minmod function is defined as

$$\text{minmod}(a,b) = \begin{cases} a, & \text{if } |a| < |b| \text{ and } ab > 0, \\ b, & \text{if } |a| > |b| \text{ and } ab > 0, \\ 0, & \text{if } ab \leq 0. \end{cases}$$

   Unfortunately, the exact solution $\tilde{u}(x,t)$, which is now a solution of a nonlinear initial value problem with piecewise linear initial data, is hard to obtain, even in the scalar

case. However, there are various ways to obtain approximate solutions which are sufficiently accurate that second order accuracy can be maintained [21], [33], [40]. By following Goodman and Osher's approach in [21], we obtain an approximation to the exact solution $\tilde{u}(x_{j+\frac{1}{2}}, t)$,

$$\tilde{u}\left(x_{j+\frac{1}{2}}(t), t\right) \approx u^*\left(\dot{x}_{j+\frac{1}{2}}(t); \tilde{U}^L_{j+1/2}, \tilde{U}^R_{j+1/2}\right),$$

where again $u^*(x/t; u_l, u_r)$ is the solution of the Riemann problem (3.15) and

$$\begin{aligned} \tilde{U}^L_{j+1/2} &= \bar{U}^n_j + \frac{(x^n_{j+1} - x^n_j)\sigma_j}{2} \\ \tilde{U}^R_{j+1/2} &= \bar{U}^n_{j+1} - \frac{(x^n_{j+1} - x^n_j)\sigma_{j+1}}{2}. \end{aligned}$$

This kind of reconstruction of the solution was extensively studied by Osher [40] in the context of fixed meshes; we call this approximation an adaptive Osher scheme.

To simplify the calculation of $\tilde{u}(x,t)$, which requires solving a sequence of Riemann problems, we require the following condition which prevents the neighboring Riemann problems from interacting:

$$x^n_{j-\frac{1}{2}} + \Delta t \cdot \max\left(f'(\tilde{U}^L_{j-\frac{1}{2}}), f'(\tilde{U}^R_{j-\frac{1}{2}})\right) \le x^n_{j+\frac{1}{2}} + \Delta t \cdot \min\left(f'(\tilde{U}^L_{j+\frac{1}{2}}), f'(\tilde{U}^R_{j+\frac{1}{2}})\right),$$

where $\tilde{U}^L_{j-\frac{1}{2}} := \lim_{x \to x^-_{j-\frac{1}{2}}} \tilde{U}$, $\tilde{U}^R_{j-\frac{1}{2}} := \lim_{x \to x^+_{j-\frac{1}{2}}} \tilde{U}$, and $\tilde{U}^L_{j+\frac{1}{2}}$ and $\tilde{U}^R_{j+\frac{1}{2}}$ are similarly defined, which leads to

$$\Delta t \le \frac{1}{2} \min_j \frac{|x^n_{j+1} - x^n_{j-1}|}{\left|\max\left(f'(\tilde{U}^L_{j-\frac{1}{2}}), f'(\tilde{U}^R_{j-\frac{1}{2}})\right) - \min\left(f'(\tilde{U}^L_{j+\frac{1}{2}}), f'(\tilde{U}^R_{j+\frac{1}{2}})\right)\right|}. \tag{3.16}$$

For a system of conservation laws, the derivatives $f'(\cdot)$ in (3.16) would be replaced by corresponding eigenvalues of the Jacobian matrix of $f(u)_x$.

Obviously, defining $\tilde{U}(x)$ in terms of higher order polynomials and approximating $\tilde{u}(x,t)$ accordingly will result in a higher order approximation [11], [24], but this is not the concern of our study.

For Burgers' equation, the Riemann problem for $u_l > u_r$ has the shock solution

$$u(x,t) = \begin{cases} u_l, & \text{if } x < st, \\ u_r, & \text{if } x > st, \end{cases}$$

where $s = (u_l + u_r)/2$. For $u_l < u_r$ one solution is given by the rarefaction

$$u(x,t) = \begin{cases} u_l, & \text{if } x < u_l t, \\ x/t, & \text{if } u_l t \le x \le u_r t, \\ u_r, & \text{if } x > u_r t. \end{cases}$$

This leads to the following definition of $u^*(x/t; u_l, u_r)$,

$$u^*(x/t; u_l, u_r) = \begin{cases} \left.\begin{array}{ll} u_l, & \text{if } s > x/t, \\ u_r, & \text{if } s < x/t, \end{array}\right\} & \text{if } u_l > u_r, \\ \left.\begin{array}{ll} u_l, & \text{if } u_l > x/t, \\ x/t, & \text{if } u_l \le x/t \le u_r, \\ u_r, & \text{if } u_r < x/t. \end{array}\right\} & \text{if } u_l < u_r, \end{cases} \tag{3.17}$$

In our computations with the adaptive Godunov scheme and the adaptive Osher scheme, this Riemann solution (3.17) will be used. For problems without an explicit Riemann solution, approximate Riemann solvers, for example, Roe's approximate Riemann problem solver [33], can be used in the place of $u^*(x/t; u_l, u_r)$.

To avoid over-resolving the shock, we modify the arclength monitor function for the moving mesh method to

$$M = \sqrt{1 + u_x^2 \cdot \exp(-\sigma \cdot |u_x|)},^{1} \tag{3.18}$$

where σ is a small parameter which controls the number of mesh points in the shock region. Notice that the modification in (3.18) makes the monitor function continuous in x even in the shock region while the arclength monitor function $\sqrt{1 + u_x^2}$ becomes discontinuous in a shock region since $u_x^2 \to \infty$.

We solve the invicid Burgers' equation (3.8) by coupling (3.14) with our moving mesh equation MMPDE6 (1.12). Two computed results shown in figures 3.8 and 3.9 are obtained with the following parameters: $\sigma = 10^{-2}$, 80 mesh points, $\tau = 10^{-2}$, $ip = 4$ indicating a 9 point smoothing, and absolute and relative error tolerance for DDASSL $rtol = atol = 10^{-6}$. The solid lines in the figures are the reference solutions obtained by a method of lines approach with Osher's scheme with 1000 fixed uniform mesh points with the same error tolerances. For the adaptive Godunov scheme, a small deviation in shock position can be observed, but bearing in mind that the Godunov scheme is a first order approximation, we consider this deviation acceptable. For the adaptive Osher scheme, the shock is perfectly resolved and its position matches with the reference solution.

[1] The author is grateful to Dr. Keith Promislow for the suggestion of this new monitor function.

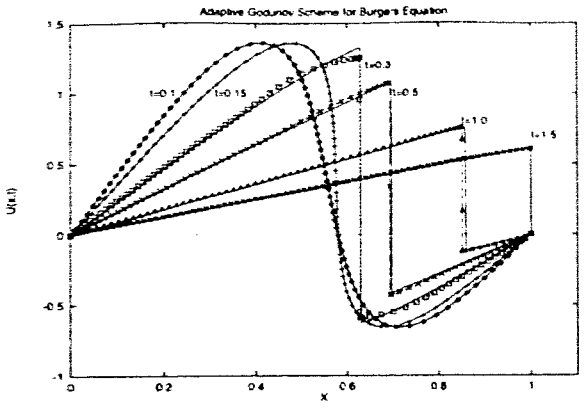

Figure 3.8: *Adaptive Godunov for invicid Burgers' equation*

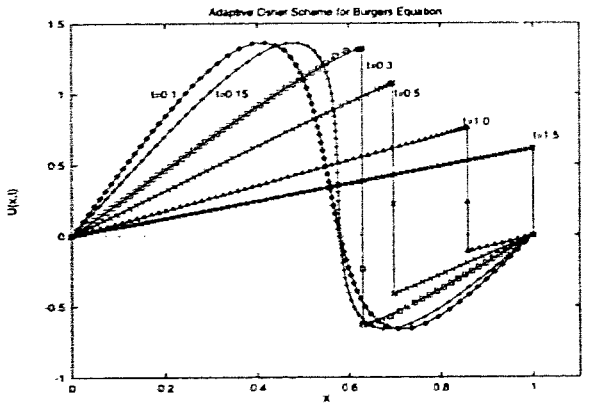

Figure 3.9: *Adaptive Osher for invicid Burgers' equation*

During the computations, we also observed $\min \Delta x \sim \sigma/10$ indicating a resolution of the shock with the magnitude $\sigma/10$, and typically $\Delta t \sim \min \Delta x/10$.

Presented in figures 3.10 and 3.11 are the mesh trajectories of a computation with the adaptive Osher scheme. As shown in figure 3.10, the modification of the monitor function (3.18) avoids over-resolving the shock by forcing some of the mesh points out of the shock region. Some mesh oscillations can also be observed indicating the necessity of a better moving mesh equation. Worth mentioning is that when the shock touches the right end of the physical interval, shown in figure 3.11, we experienced some very small time steps ($\sim 10^{-8}$). The possible reason for this phenomenon is that we need spatial smoothing (a 9-point averaging is used here) to regularize the distribution of the mesh points, and when there are only a few points (say, < 4) left before the shock, where the monitor function takes large value, more time steps are needed to propagate the information about the monitor

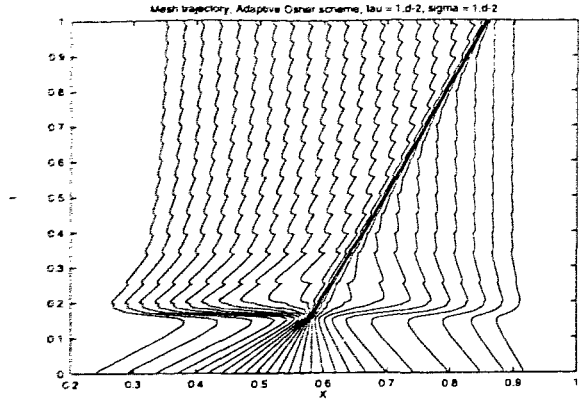

Figure 3.10: *Mesh trajectory of adaptive Osher scheme,* $0 < t < 1$

function to other mesh points so as to move the mesh points backward. The time integration also takes a few small steps when a mesh point needs to be moved out of the shock region, e.g., near the blowup time when u_x begins to approach infinity.

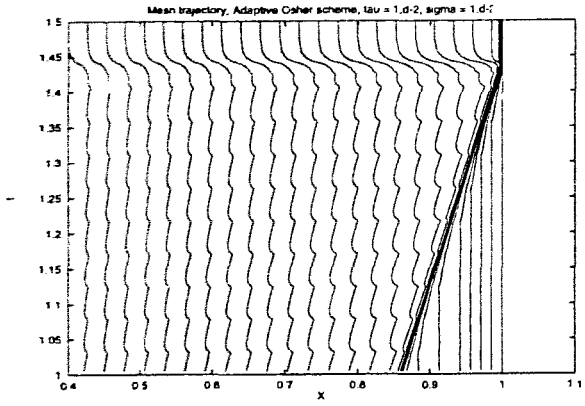

Figure 3.11: *Mesh trajectory of adaptive Osher scheme,* $1 < t < 1.5$

Typical performance of the method for the time period $0 < t < 1$ is summarized in table 3.2 where the column N contains the number of mesh points used, NTS contains the number of time steps, RES contains the number of residue evaluations, JAC contains the number of Jacobian evaluations, and CPU contains the computer time used for the computation. Compared with a fixed mesh method of lines approach, which is used to obtain the reference solution, our method is reasonably more efficient to reach the same resolution of the shock, but the new method is less efficient compared with previous moving mesh computations *with* artificial viscosity terms [29]. However, our emphasis in this study is to show how to compute a possibly discontinuous solution with the moving mesh method.

	N	τ	σ	$\min \Delta x$	NTS	RES	JAC	CPU
Fixed Mesh Osher (MOL)	1000			10^{-3}	8232	13581	1774	1660
Adaptive Godunov	80*	10^{-2}	10^{-2}	$\sim 10^{-3}$	2829	4952	345	52
		10^{-3}	10^{-2}	$\sim 10^{-3}$	3463	6423	479	69
		10^{-4}	10^{-2}	$\sim 10^{-3}$	3879	7762	740	96
		10^{-5}	10^{-2}	$\sim 10^{-3}$	4544	9173	998	122
		10^{-2}	10^{-3}	$\sim 10^{-4}$	14688	24858	6378	642
Adaptive Osher	80†	10^{-2}	10^{-2}	$\sim 10^{-3}$	3171	5429	328	61
		10^{-2}	10^{-3}	$\sim 10^{-4}$	13392	22194	4263	523
	100	10^{-2}	10^{-2}	$\sim 10^{-3}$	3850	6509	406	102
		10^{-2}	10^{-3}	$\sim 10^{-4}$	13016	20342	1686	360

Table 3.2: *Performance comparison of fixed mesh computation and Godunov approach, *: shown in figure 3.8; †: shown in figure 3.9.*

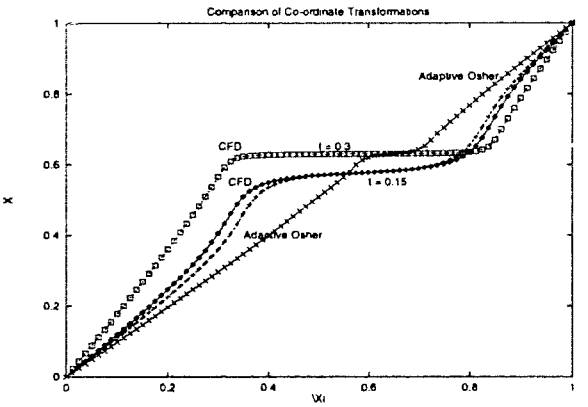

Figure 3.12: *Comparison of co-ordinate transformations*

In figure 3.12, we compare the coordinate transformation, dictated by the new monitor function (3.18) with $\sigma = 10^{-2}$, of a computation with the adaptive Osher scheme for inviscid Burgers' equation (3.8) and that, dictated by the arclength monitor function $M = \sqrt{1 + u_x^2}$, of a computation with a centered finite difference (CFD) scheme for viscid Burgers' equation (3.9) with $\epsilon = 10^{-3}$. At time $t = 0.15$ (before the blowup time), the two transformations are almost the same. After the formation of the shock ($t = 0.3$) the new approach put only a few mesh points in the shock region while the CFD computation moves more mesh points into the shock region to keep the computation stable as implied by (3.12).

3.3 Summary and Discussion

In this chapter, we study the conservation laws with the method of lines approach and moving mesh methods. It is shown that with the finite difference approach an important feature of the moving mesh method is to provide viscosity adaptively, and for viscous conservation laws with centered finite difference discretization the moving mesh methods are, implicitly, equivalent to adaptive viscosity methods.

Although proven to be successful and efficient for some problems, moving mesh methods based on moving mesh PDEs should, in general, be used with caution. For certain problems not all spatial discretization are permissible.

A new Godunov type approach for conservation laws with adaptive meshes is developed and shown to be successful in shock resolution. Although improvement in efficiency may be required, it shows the potential of moving mesh methods for conservation laws.

For problems without explicit Riemann solutions, an approximate Riemann problem solver can be used to approximate $\tilde{u}(x,t)$ in (3.14), and a new moving mesh equation may be required to improve both the accuracy and efficiency. Notice that we had used a linear (first order) approximation for $x_{j+\frac{1}{2}}(t)$ in the derivation of the methods. One possible improvement may be to define a moving mesh equation such that

$$\dot{x}_{j+\frac{1}{2}}(t) = c^n_{j+\frac{1}{2}}, \quad t_n < t < t_n + \Delta t,$$

where $c^n_{j+\frac{1}{2}}$ is a constant in the interval $t_n < t < t_n + \Delta t$ which depends on the solution profile at time $t = t_n$, perhaps selected by equipartition of some monitor function. Such a method could be more accurate. This approach may also lead to improvement in efficiency with this redefinition of the moving mesh equation.

In principle, the idea of cell averaging can be used in higher dimensional cases with some additional difficulties. The approximation to the exact Riemann solution may provide clues for possible moving mesh equations in higher dimensions.

Chapter 4

Concluding Remarks

In this thesis, we studied blowup problems and conservation laws with moving mesh methods based on MMPDEs.

For blowup problems, basically reaction-diffusion equations, moving mesh methods are successful. The computational results agree with our analysis. Due to the problem-independent nature of the moving mesh equations, a properly chosen monitor function, which preserves the invariant property of the physical equation, is required for the success of the computations. We show that the blowup point and time can be accurately captured by moving mesh methods.

A formal analysis is carried out for a blowup system. The relationship between the two components is confirmed by the computations. Our computations also show that, with proper monitor function, moving mesh methods can automatically distinguish between blowup and nonblowup solutions. Thus moving mesh methods are ideal for studying blowup problems. Moving mesh methods are used to compute the solution of a problem with blowup in a set. The results provide an accurate description of the blowup behavior.

A finite difference approach for viscous conservation laws was shown to be successful. Our analysis shows that, for viscous conservation laws, with centered finite difference discretization, moving mesh methods implicitly adapt the artificial viscocity. But proper spatial discretization is cruicial for the success of the computations. With varied centered finite difference, which is one order higher for nonuniform meshes, the method fails to give correct shock speed and fails to preserve stability. Although an increase of the parameter τ will increase the time step, it is impossible to keep the computation stable without the artificial viscocity. For invicid conservation laws, the time step could be too small to be

practicable and some artificial viscocity is necessary. When moving mesh methods are used with invicid conservation laws, the mesh distribution becomes too far away from uniform and the analysis becomes much more complicated.

Generally speaking, caution must be taken when moving mesh methods are to be used. An *a priori* error analysis for different spatial discretizations may be very helpful and ofter necessary.

New adaptive Godunov type schemes for conservation laws are developed and they are shown to be successful in efficiency and shock resolution. Further development in this direction is a good topic for future study.

Bibliography

[1] S. Adjerid and J. E. Flaherty, "A Moving-Mesh Finite Element Method with Local Refinement for Parabolic Partial Differential Equations." *Comput. Meth. in Appl. Mech. Engng.* **55**, 3 – 26, 1986.

[2] D. A. Anderson, "Adaptive mesh schemes based on Grid Speeds", AIAA Paper, **83 – 1931** , p. 311, 1983.

[3] U. M. Ascher, R. M. M. Mattheij, R. D. Russell, "Numerical Solutions of Boundary Value Problems for Ordinary Differential Equations", Prentice-Hall Inc., 1988

[4] M. J. Baines, "Moving Finite Elements", Oxford Science Publications, Clarendon Press, Oxford, 1994.

[5] R. E. Bank and R. F. Santos, "Analysis of Some Moving Space-Time Finite Element Methods", *SIAM J. Numer. Anal.*, Vol. **30**, No. 1, p. 1, 1993.

[6] M. Berger and R. V. Kohn, "A Rescaling Algorithm for the Numerical Calculation of Blowing-up Solutions", *Comm. Pure Appl. Math.*, Vol. **XLI**, 841 – 863, 1988.

[7] J. Bell, "Three-Dimensional Adaptive Mesh Refinement for Hyperboic Conservation Laws", *SIAM J. Sci. Comput.*, Vol. **15**, No. 1, 127 – 138, 1994.

[8] R. Biswas, K. D. Devine, and J. E. Flaherty, "Parallel, Adaptive Finite Element Methods for Conservation Laws", *Trans. of App. Num. Math.*, Vol. **14**, No. **1/3**, p.255, 1994.

[9] de Boor, "Good Approximation by Splines with Variable Knots II", in Springer Lecture Notes Series **363**, Springer-Verlag, Berlin, 1973.

[10] C. J. Budd, W. Huang, and R. D. Russell, "Moving Mesh Methods for Problems with Blow-Up", *SIAM J. Sci. Comput.*, Vol. **17**, No. **2**, p. 305, 1996.

[11] P. Colella and P. Woodward, "The Piecewise-Parabolic Method (PPM) for Gas-Dynamic Simulations", *J. Comput. Phys.*, **54**, 174 – 201, 1984.

[12] J. M. Coyle, J. E. Flaherty, and R. Ludwig, "On the Stability of Mesh Equidistribution Strategies for Time-Dependent Partial Differential Equations", *J. Comput. Phys.*, **62**, 26 – 39, 1986.

[13] D. S. Dodson, "Optimal order approximation by Polynomial Spline Functions", Ph.D. thesis, Purdue University, West Layfette, IN, 1972.

[14] E. A. Dorfi and L. O'c. Drury, "Simple Adaptive Grids for 1-D Initial Value Problems", *J. Comput. Phys.*, **69**, 175 – 195, 1987.

[15] M. Escobedo and M. A. Herrero, "Boundedness and Blow Up for a Semilinear Reaction-Diffusion System", *J. Diff. Equ.*, **89**, 176 – 202, 1991.

[16] J. E. Flaherty, J. M. Coyle, R. Ludwig, and S. F. Davis, "Adaptive Finite Element Methods for Parabolic Partial Differential Equations", in *Adaptive Computational Methods for Partial Differential Equations*, I. Babuška, J. Chandra, and J. E. Flaherty, eds., Society for Industrial and Applied Mathematics, Philadelphia, PA, 144 – 164, 1983.

[17] M. S. Floater, "Blow-up at the Boundary for Degenerate Semilinear Parabolic Equations", *Arch. Rational Mech. Anal.*, **114**, 57 – 77, 1991.

[18] R. M. Furzeland, J. G. Verwer and P. A. Zegeling, "A Numerical Study of Three Moving Grid Methods for One-Dimensional Partial Differential Equations Which Are Based on the Method of Lines.", *J. Comput. Phys.* **89**, 349 – 388, 1990.

[19] V. A. Galaktionov, "On a Blow-Up Set for the Quasilinear Heat Equation $u_t = (u^\sigma u_x)_x + u^{\sigma+1}$", *J. Diff. Equ.*, **101**, 66 – 79, 1993.

[20] V. A. Galaktionov, S. P. Kurdyumov, A. P. Mikhailov, and A. A. Samarskii, "On Unbounded Solutions of the Cauchy Problem for Parabolic Equation $u_t = \nabla(u^\sigma \nabla u) + u^\beta$", *Dokl. Akad. Nauk. SSSR Ser. Math.*, **252**, 1362 – 1364, 1980 (in Russian).

[21] J. B. Goodman and R. J. LeVeque, "A Geometric Approach to High Resolution TVD Schemes", *SIAM J. Num. Anal.*, Vol. **25**, No. **2**, 268 – 284, 1988.

[22] B. F. Gray and S. K. Scott, "The influence of initial temperature excess on critical conditions for thermal explosion", *Combustion and Flames*, **61**, 227 – 237, 1985.

[23] A. Harten and J. M. Hyman, "Self-Adjusting Grid Methods for One-Dimensional Hyperbolic Conservation Laws", *J. Comput. Phys.*, **50**, 235 – 269, 1983.

[24] A. Harten and S. Osher, " Uniformly High-Order Accurate Nonoscilatory Schemes. I", *SIAM J. Num. Anal.*, **24**, 279 – 309, 1987.

[25] D. F. Hawken, J. J. Gottlieb and J. S. Hansen, "Review of Some Adaptive Node-Movement Techniques in Finite Element and Finite Difference Solutions of PDEs", *J. Comput. Phys.*, **95**, 254 – 302, 1991.

[26] B. M. Herbst, S. W. Schoombie, and A. R. Mitchell,"Equidistributing Principles in Moving Finite Element Methods", *J. Comput. Appl. Math.*, **9**, 377 – 389, 1983.

[27] R. G. Hindman and J. Spencer, "A New Approach to Truly Adapeive Grid Generation", *AIAA Paper* **83 – 0450** , p. 1, 1983.

[28] W. Huang, Y. Ren, and R. D. Russell, "Moving Mesh Partial Differential Equations (MMPDEs) Based on the Equidistribution Principles", *SIAM J. Numer. Anal.*, Vol. **31**, No. **3**, 709 – 730. 1994.

[29] W. Huang, Y Ren, and R. D. Russell, "Moving Mesh Methods Based on Moving Mesh Partial Differential Equations", *J. Comput. Phys.*, **112**, 279 – 290, 1994.

[30] W. Huang and R. D. Russell, "Analysis of Moving Mesh Partial Differential Equations with Spatial Smoothing", to appear in *SIAM J. Sci. Comput.*.

[31] W. Huang and R. D. Russell, "MOVCOL, A MOVing COLlocation Code for Solving Second-Order Parabolic Partial Differential Equations", *Appl. Numer. Math.*, Vol. **20**, 101 – 116, 1996.

[32] J. M. Hyman, "Adaptive Moving Mesh Methods for Partial Differential Equations", in ***Advances in Reactor Computations***, American Nuclear Society Press, La Grange Park, IL, 1983, 24 – 43.

[33] R. J. LeVeque, "Numerical Methods for Conservation Laws", Birkhäuser Verlag, Basel, 1992.

[34] S. Li, L. Petzold, and Y. Ren, "Stability of Moving Mesh Systems of Partial Differential Equations", to appear.

[35] B. J. Lucier, "A Stable Adaptive Numerical Scheme for Hyperbolic Conservation Laws", *SIAM J. Num. Anal.*, Vol. **22**, No. **1**, 180 – 203, 1985.

[36] K. Miller and R. N. Miller, "Moving Finite Elements I", *SIAM J. Numer. Anal.*, **18**, 1019 – 1032, 1981.

[37] K. Miller,"Moving Finite Elements II", *SIAM J. Numer. Anal.* **18**, 1033 – 1057, 1981.

[38] K. Miller, in *Accuracy Estimates and Adaptive Refinements in finite Element Computations*, edited by I. Babuška, O. C. Zienkiewicz, Z. Gago, and E. R. de A. Oliveira (Wiley, New York, 1986), p. 325.

[39] H. Ockendon, "Channel Flow with Temperature-Dependent Viscosity and Internal Viscous Dissipation", *J. Fluid Mech.*, **93**, 737 – 746, 1979.

[40] S. Osher, "Convergence of Generalized MUSCL schemes", *SIAM J. Num. Anal.*, **22**, 947 – 961, 1985.

[41] L. R. Petzold, "A Description of DASSL: A Differential/Algebraic System Solver", SAND82-8637, Sandia Labs, Livermore, Cal., 1982.

[42] L. R. Petzold, "Observations on an Adaptive Moving Grid Method for One-Dimensional Systems of Partial Differential Equations", *App. Numer. Math.*, **3**, 347 – 360, 1987.

[43] A. B. White, Jr., "On Selection of Equidistributing Meshes for Two-Point Boundary-Value Problems", *SIAM J. Numer. Anal.*, **16**, 1265 – 1286, 1979.

[44] Yuhe Ren, "Theory and Computation of Moving Mesh Methods for Solving Time-Dependent Partial Differential Equations", Ph. D. thesis, Simon Fraser University, Burnaby, B.C., Canada, 1991.

[45] Yuhe Ren and R. D. Russell, "Moving Mesh Techniques Based upon Equidistribution, and Their Stability", *SIAM J. Sci. Stat. Comput.*, Vol. **13**, No. **6**, 1265 – 1286, Nov. 1992.

[46] R. D. Russell and J. Christiansen, "Adaptive Mesh Selection Strategies for Solving Boundary Value Problems", *SIAM J. Numer. Anal.*, **15**, 59 - 80, 1987.

[47] W. E. Schiesser "The Numerical Method of Lines: Integration of Partial Differential Equations", Academic Press, 1991

[48] P. A. Zegeling and J. G. Blom, "An evaluation of the Gradient-Weighted Moving-Finite-Element Method in One Space Dimension", *J. Comput. Phys.*, Vol. **103**, No. **2**, p. 422, 1992